PSU Aersb 73-7

# AN ANALYTICAL AND EXPERIMENTAL STUDY OF FARFIELD ROTOR WAKE GEOMETRY AND VELOCITY

by

Thomas Alan Egolf

Performed Under U. S. Army Contract
DA-ARO D-31-124-71-G13

Department of Aerospace Engineering
The Pennsylvania State University
University Park, Pa.

August 1973

DOCUMENT CONTROL DATA - R & D

*(Security classification of title, body of abstract and indexing annotation must be entered when the overall report is classified)*

| 1. ORIGINATING ACTIVITY (Corporate author) | 2a. REPORT SECURITY CLASSIFICATION |
|---|---|
| Pennsylvania State University | Unclassified |
| | 2b. GROUP NA |

3. REPORT TITLE

AN ANALYTICAL AND EXPERIMENTAL STUDY OF FARFIELD ROTOR WAKE GEOMETRY AND VELOCITY

4. DESCRIPTIVE NOTES (Type of report and inclusive dates)

Technical Report

5. AUTHOR(S) (First name, middle initial, last name)

Thomas Alan Egolf

| 6. REPORT DATE | 7a. TOTAL NO. OF PAGES | 7b. NO. OF REFS |
|---|---|---|
| August 1973 | 64 | |

| 8a. CONTRACT OR GRANT NO. | 9a. ORIGINATOR'S REPORT NUMBER(S) |
|---|---|
| DA-ARO-D-31-124-71-G13; 73-G36 | |
| b. PROJECT NO. | NA |
| c. | 9b. OTHER REPORT NO(S) (Any other numbers that may be assigned this report) |
| d. | ARO - 9334.3-E |

10. DISTRIBUTION STATEMENT

Approved for public release; distribution unlimited.

| 11. SUPPLEMENTARY NOTES | 12. SPONSORING MILITARY ACTIVITY |
|---|---|
| None | U. S. Army Research Office<br>Box CM, Duke Station<br>Durham, North Carolina 27706 |

13. ABSTRACT

All fixed wing aircraft generate trailing vortex wakes whose circulatory strength is dependent on flight conditions and aircraft geometry. A rotor also generates a vortex wake. A vortex sheet is shed from each blade. Each sheet rolls up rapidly outboard to form a tip vortex. The purpose of the study reported here is to estimate the rotor wake geometry and velocity field downstream of the rotor for the particular case where the rotor wake exhibits strong similarities to the fixed wing wake. A method is developed by which the helicopter far field wake can be readily compared to the far field wake generated by an equivalent wing.



14. KEY WORDS

Rotor wakes
Rotary wings
Vortices
Wake geometry





DD FORM 1 NOV 68 1473 REPLACES DD FORM 1473, 1 JAN 64, WHICH IS OBSOLETE FOR ARMY USE.

PSU Aers P-73-7

The Pennsylvania State University

The Graduate School

Department of Aerospace Engineering

# AN ANALYTICAL AND EXPERIMENTAL STUDY OF FARFIELD ROTOR WAKE GEOMETRY AND VELOCITY

A Thesis in

Aerospace Engineering

by

Thomas Alan Egolf

Submitted in Partial Fulfillment
of the Requirements
for the Degree of

Master of Science

August 1973

Approved:

Barnes W. McCormick, Professor and Head, Department of Aerospace Engineering, Thesis Advisor

Joseph J. Eisenhuth, Associate Professor of Aerospace Engineering

# ACKNOWLEDGMENTS

The author wishes to thank his graduate advisor, Dr. Barnes W. McCormick, Jr., for his guidance and assistance in the preparation of this thesis. Sincere thanks are also extended to Mr. Gerald F. Hall for his time, patience, and aid in many phases of this study, and to Mr. Edward P. Jordan for his assistance in many of the technical aspects of this project. This study was sponsored by the U. S. Army Research Office - Durham under Contract No. DA-ARO-D-31-124-71-613.

# TABLE OF CONTENTS

# NOMENCLATURE

Roman

| | |
|---|---|
| $a$ | Core radius of a vortex |
| $a_1$ | Longitudinal flapping parameter |
| $a_o$ | Slope of the rotor airfoil section lift curve |
| $A_f$ | Amplification factor; $\Gamma_\infty/\Gamma_o$ |
| $b_1$ | Lateral flapping parameter |
| $B$ | Number of rotor blades |
| $c$ | Chord of a wing or rotor blade |
| $C_L$ | Rotor lift coefficient; $T/\frac{1}{2}\rho V^2 \pi R^2$ |
| $C_T$ | Thrust coefficient; $T/\rho V_T{}^2 \pi R^2$ |
| $D$ | Drag of a helicopter in flight |
| $h$ | Perpendicular distance from a vortex filament to any point in space; or non-dimensional hub radius |
| $\tilde{i},\tilde{j},\tilde{k}$ | Unit vectors in x,y,z directions respectively |
| $I_1$ | Blade moment of inertia |
| $k$ | Constant of proportionality; $\Gamma(a)/\Gamma_\infty$ |
| $L$ | Lift of a wing or rotor |
| $M_w$ | Blade weight moment |
| $\tilde{p}$ | Non-dimensional vector from any point to a point on a vortex |
| $R$ | Rotor radius or wing semi-span |
| $\tilde{s}$ | Non-dimensional vector describing vortex location |
| $t$ | Time |
| $T$ | Thrust of a rotor |
| $T_B$ | Non-dimensional radial position on rotor blade to account for tip losses |
| $v$ | Induced velocity at any point |
| $\tilde{v}$ | Induced velocity vector at any point |

NOMENCLATURE (continued)

| | |
|---|---|
| $v_i$ | Maximum induced tangential velocity |
| V | Forward flight speed |
| $V_T$ | Tip speed of a rotor |
| w | Downwash of the rotor |
| W | Weight of helicopter |
| x | Non-dimensional station on rotor blade or downstream coordinate, positive in downstream position |
| $x_o$ | x coordinate at a point |
| y | Coordinate in spanwise direction, positive by rule convention |
| $y_o$ | y coordinate at a point |
| z | Coordinate in vertical direction, positive upward |

Greek

| | |
|---|---|
| $\alpha$ | Angle of attack of rotor disk plane |
| $\beta$ | One of two interval angles defined by a vortex filament of finite length and any point |
| $\beta_o$ | Coning angle |
| $\gamma$ | One of two interval angles defined by a vortex filament of finite length at any point |
| $\Gamma$ | Circulation of a vortex filament |
| $\Gamma_B$ | Total circulation of tip vortex and/or bound circulation at the rotor tip |
| $\Gamma_o$ | Product of the number of blades and the tip vortex circulation |
| $\Gamma_\infty$ | Total circulation of a vortex on the mid-span bound circulation |
| $\Gamma_1, \Gamma_2, \Gamma_3$ | Circulation parameters |
| $\Gamma^*$ | Non-dimensional circulation |
| $\Gamma(a)$ | Circulation at the core radius |

NOMENCLATURE (continued)

| | |
|---|---|
| $\Gamma(x)$ | Bound circulation at any x station on a rotor blade |
| $\theta_o$ | Hub collective pitch angle |
| $\lambda$ | Inflow ratio |
| $\mu$ | Tip speed ratio |
| $\rho$ | Density of air |
| $\sigma$ | Rotor solidity, $Bc/\pi R$ |
| T | Period of rotor blade revolution |
| $\phi$ | Azimuthal position of blade at time t = 0 |
| $\psi$ | Azimuthal position of blade at any time ($-\omega t$) |
| $\omega$ | Angular velocity of rotor |

# LIST OF TABLES

# LIST OF FIGURES

# LIST OF FIGURES

# CHAPTER I

## INTRODUCTION

All fixed wing aircraft generate trailing vortex wakes whose circulatory strength is dependent on flight conditions and aircraft geometry. Large heavy airplanes can generate extremely strong trailing vortex systems during landing approaches, takeoffs, or other low speed flight conditions. Wetmore and Reeder[1] and many others have studied this problem as it applies to aircraft terminal operations, and it is well established that lighter and smaller aircraft can be severely affected by encounters with these strong vortex wakes. When this occurs the aircraft ordinarily experiences severe rolling or pitching moments, or a combination of both, depending on the aircraft attitude with respect to the vortex system. These moments may cause loss of control or structural damage to the aircraft. If the aircraft is centered between the trailing vortices of a larger airplane it may experience a severe down draft. Although larger aircraft are not as strongly affected by these vortices, large rolling moments can still be developed which could be disasterous during low altitude flight.

These vortices, being in a real fluid, have a central region of rotational motion defined as a vortex core. McCormick[2], Hoffman and Joubert[3], Spreiter and Sacks[4], and others have studied the problem of predicting the geometry of a vortex. As a result, a great deal of information has been assembled concerning vortex geometry and behavior.

The trailing vortices of a fixed-wing aircraft are formed when the vortex sheet shed from the wing rolls up downstream into two discreet vortices located inboard from each wing tip. As noted by McCormick[2],

and many others, this roll up is quite rapid and occurs within two or three chord lengths of the wing trailing edge. The two vortices rotate in opposite directions but with the same circulatory strength. For a wing the circulatory strength of these vortices is the midspan value of the bound circulation on the wing. Figure 1 is a sketch of the roll-up of the vortex sheet shed from a wing in forward flight. Each vortex induces a velocity on the other causing the vortex system to move downward at a constant rate until the system decays or meets a boundary such as an airport runway, at which time the two vortices spread out laterally along the surface until they decay.

A rotor also generates a vortex wake. A vortex sheet is shed from each blade. Each sheet rolls up rapidly outboard to form a tip vortex. The inboard sheet never coalesces into a strong vortex system and from Lehman's[5] studies of rotor flow patterns, it appears to have no effect on the far field wake configuration. There are basically three types of far field wake configurations which the tip vortices then form, all being variations of a helical trail whose boundaries are defined by a skewed elliptical cylinder. Lehman's studies of rotor flow patterns clearly show the characteristics of each type. Referring to Figure 2, the first pattern is characterized by nearly vertical helical vortex trails, which occur at low tip speed ratios. The second type of pattern occurs at moderate tip speed ratios where the skew angle is becoming large. The tip vortices combine to form two oppositely rotating vortices similar to a fixed wing vortex system. The final configuration is that of a coarsely pitched, highly skewed helix. It generally occurs at high tip speed ratios and large skew angles. Figure 3 is an illustration of the similarities between the fixed-wing and rotor wakes.

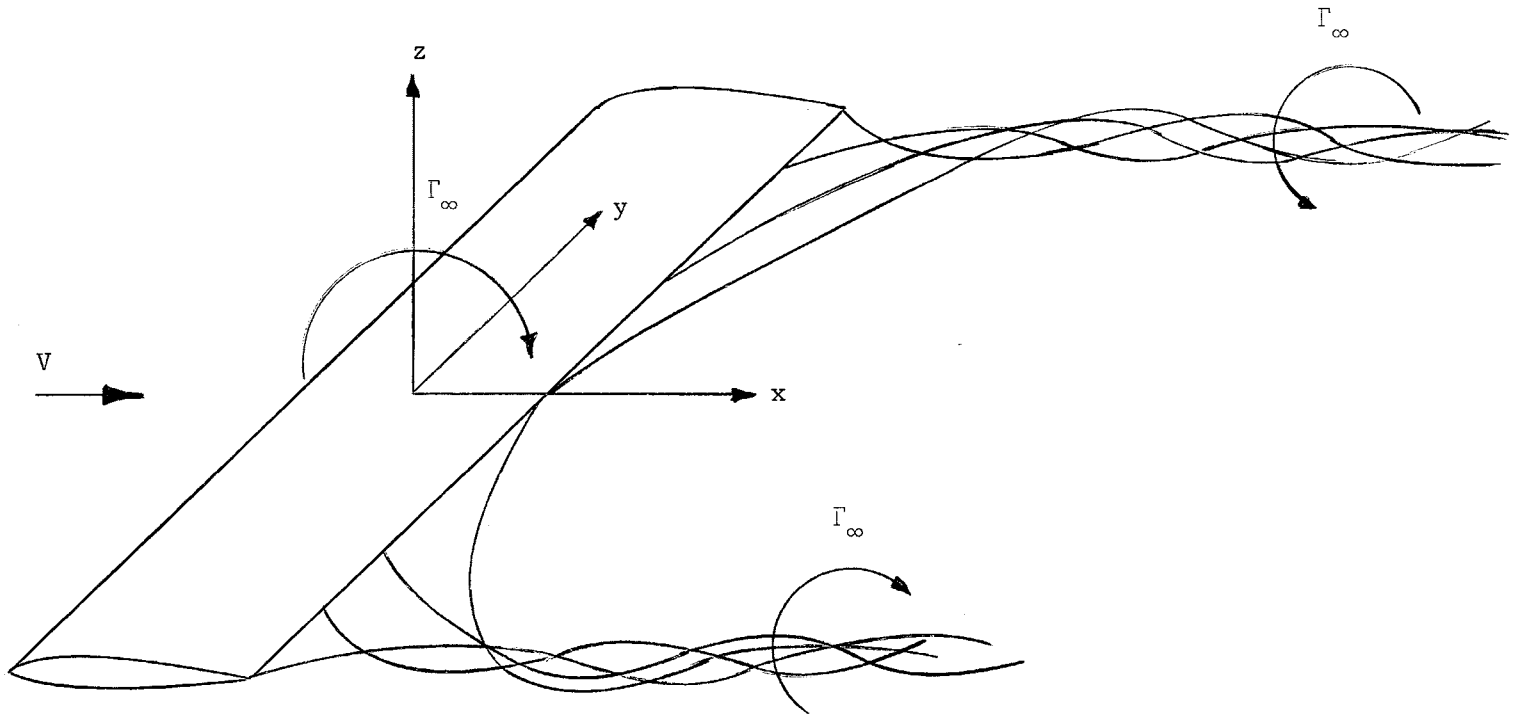


Figure 1. Typical Trailing Vortex System of a Fixed Wing.

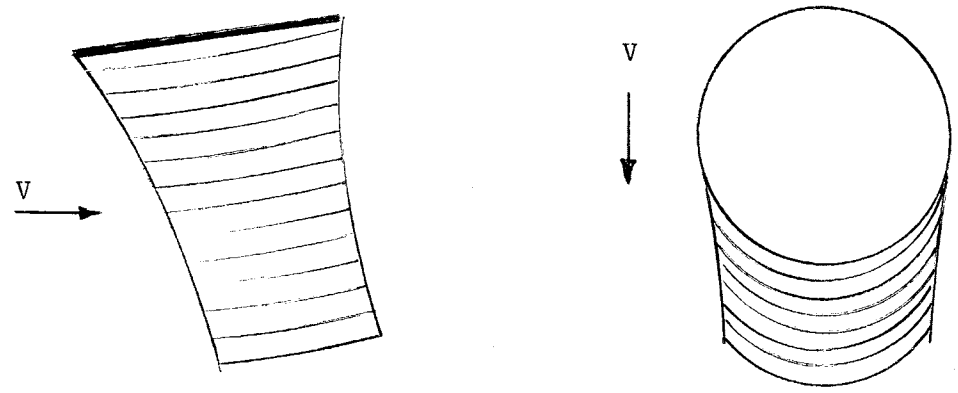


a) Low Tip Speed Ratios

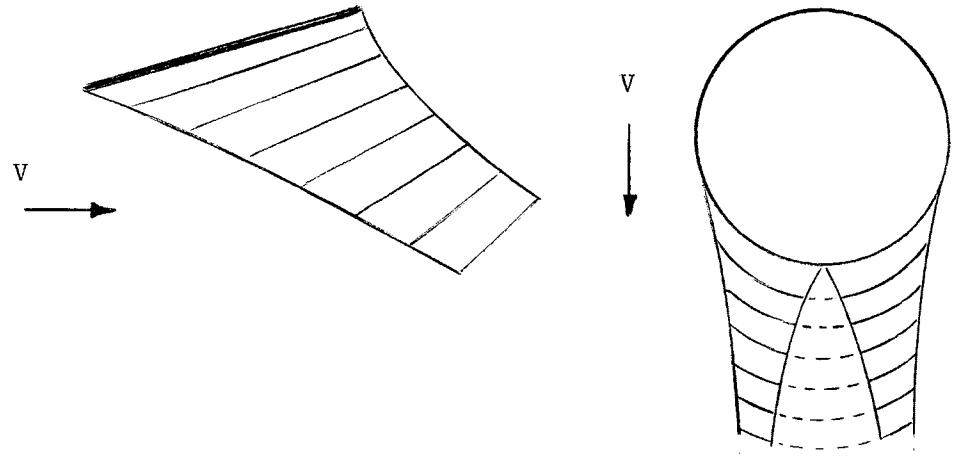


b) Moderate Tip Speed Ratios

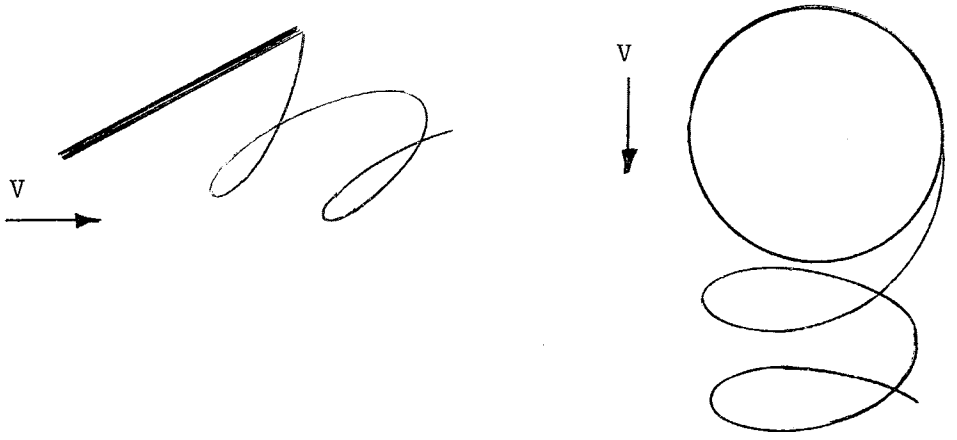


c) High Tip Speed Ratios

Figure 2. Three Types of Rotor Wake Configurations.

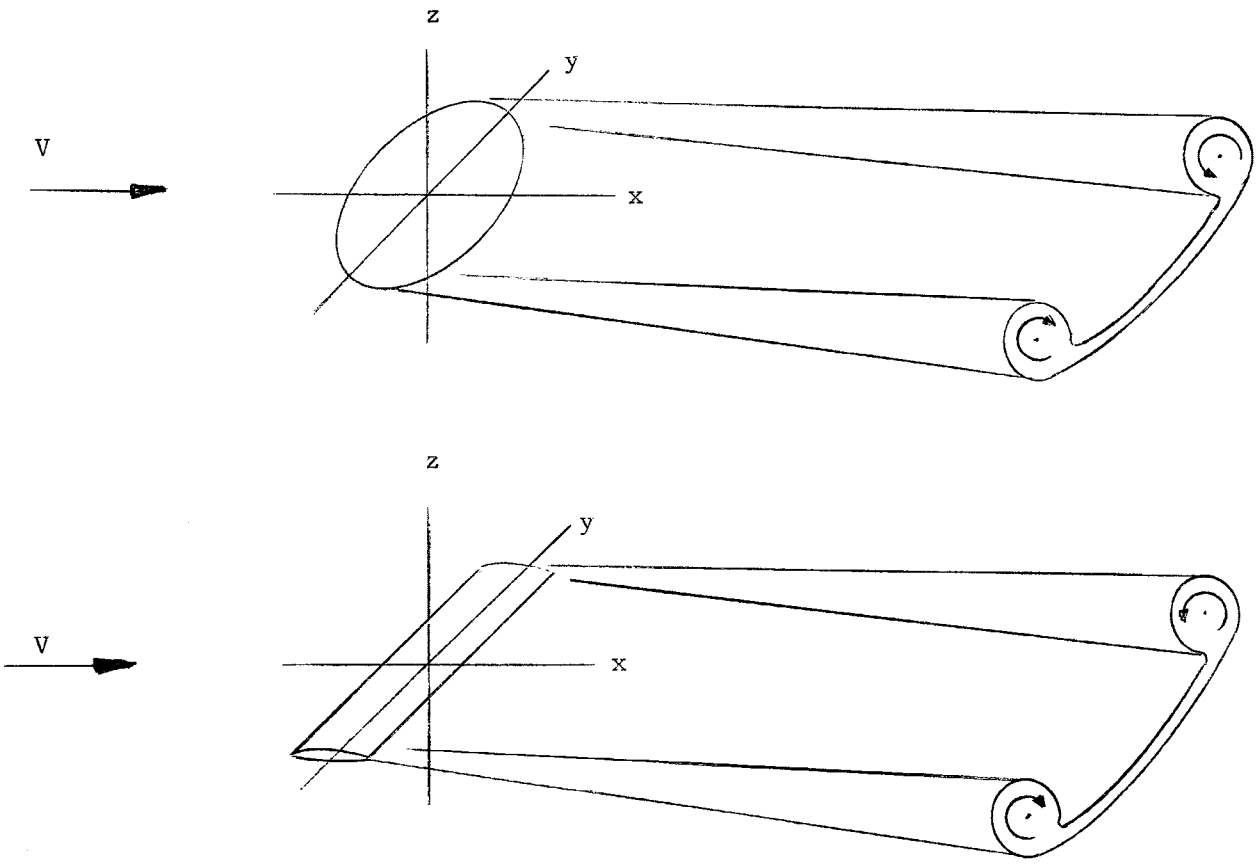


Figure 3. Similarity Between Rotor and Fixed Wing Farfield Wakes.

The purpose of this study is to estimate the rotor wake geometry and velocity field downstream of the rotor for the particular case where the rotor wake exhibits strong similarities to the fixed-wing wake. A method is developed by which the helicopter far field wake can be readily compared to the far field wake generated by an equivalent wing. With this method an estimate of helicopter wake decay can be made based on work done by McCormick, Tangler, and Sherrieb[2] for trailing vortices of conventional aircraft.

The conventional methods of predicting rotor wake geometry and velocity fields in forward flight by the use of analytical models are reasonably accurate in predicting blade loadings and time varying flow fields in the vicinity of the rotor. Landgrebe[6], Heyson[7], and Crimi[8], to name a few, have done significant work in this area. These methods, however, are not applicable far downstream from the rotor because they do not consider real fluid effects in the wake which must be considered in predicting the geometry of the wake. They also involve time consuming computer programs whose accuracy is unnecessary for far field wake predictions.

An early study using a smoke visualization technique and a hot-wire anemometer to measure and locate rotor blade tip vortices was done by Simons, Pacifico, and Jones[9]. Their study indicated that the outboard shed vortex sheet was fully rolled up within one rotor radius. This result is clearly validated by pictorial results from a later study done by Lehman[10] concerning model helicopter rotors.

Landgrebe[6] and Crimi[8] use distorted wake models to calculate blade loads and near field velocities. Both of these analytical models have shown the tendency for the modeled rotor wake to begin rolling up

into two trailing vortices downstream from the rotor. Heyson's[7] model for a rotor wake is an undistorted classical model. Although the wake geometry is fixed, the downstream velocity field appears to be similar to a fixed-wing wake velocity field. In a later publication with most of the same information, Heyson[11] compares measured velocities downstream from the rotor, which occur between the center of the two trailing vortices in the plane of the vortices, with calculated velocities based on a model for a fixed-wing far field wake. He obtained reasonable results, but the model presented was only designed for calculating the center line velocities. Heyson's measured velocities behind an actual large scale model rotor also clearly show the similarities between the rotor and fixed-wing far field wake. The tip vortex systems generated by Heyson's[9] large scale model always rolled up into two trailing vortices within a rotor radii. One of the conclusions that Heyson made from the results of his study was that the far field rotor wake could be modeled more accurately by a wing than a rotor if the rotor lift coefficient is sufficiently high.

There have been some studies done on the aircraft-helicopter wake interaction problem; one such study was done by Connor and O'Bryan[12]. Their study consisted basically of flight tests with an airplane and helicopter. The results of their study indicated that helicopter wakes presented potential hazards to aircraft operating in the vicinity of the helicopter. They suggested that a separation interval of about one minute between helicopter and airplanes would be sufficient for safe operation of the airplane for their particular generation of helicopters. It should be noted however that their report is over a decade old. Today, helicopters with high payload capacities are much larger than

they were ten years ago, indicating that the helicopter vortex-airplane interaction is now a more serious problem.

A general approach to the problem of estimating far field rotor wake geometry and velocities is described below. Both analytical methods and experimental data are incorporated in this study. In addition to Heyson's[9] measured data for a large scale rotor, measurements were made behind a model rotor by the author.

Several different analytical approaches will follow. First, a gross treatment of the rotor is made, whereby the rotor disk is considered to be a low aspect ratio elliptic wing. Geometric considerations are then presented to estimate the trailing vortex strength. Next, a fixed wake model of the tip vortices is numerically integrated to obtain velocity fields for various operating conditions. These velocity fields are also used to estimate the effective trailing strength. Finally, an analysis of the rotor wake circulatory strength is made by using an analytical model of a flapping rotor in forward flight.

With the results from the above analyses, together with experimental data, the relationship between the rotor and an equivalent wing are established. This relationship can then be used in conjunction with Reference 2 to model the helicopter far field wake.

# CHAPTER II

# ANALYSIS

## A Gross Treatment of the Rotor Disk as a Wing

An elliptic wing of semi-span R with a flight speed of V would have a mid-span bound circulation of $\Gamma_\infty$, given by

$$\Gamma_\infty = \frac{2L}{\pi\rho VR} \tag{1}$$

Assuming a thrusting rotor with a rotor radius of R, and a flight speed of V, to be analogous to the elliptic wing, the total circulatory strength of the trailing vortices would be:

$$\Gamma_\infty = \frac{2T}{\pi\rho VR} \tag{2}$$

The circulation at the core radius of a vortex has been shown by McCormick et al.[2] to be linearly proportional to the total circulation of the vortex.

$$\Gamma(a) = k\,\Gamma_\infty \tag{3}$$

The constant of proportionality k, is dependent on the nature of the vortex. For small scale wing models k has a value of .716, which comes from a solution of the Navier-Stokes equations. For large scale wings and real aircraft k has a value of approximately 0.16. This value results from empirical measurements presented in Reference 2. This reference also shows that the circulation of large scale vortices follows a logarithmic distribution as presented by Hoffman and Joubert[3].

The rotor lift coefficient will be defined as the rotor thrust divided by the free stream dynamic pressure and disk area.

$$C_L = \frac{T}{1/2\rho V^2 \pi R^2} \tag{4}$$

Analysis of Grow's[13] data on the maximum induced tangential velocity of a trailing vortex shows that the maximum velocity is proportional to the wing lift coefficient and free stream velocity. The constant of proportionality is independent of aspect ratio for aspect ratios greater than 4, with a value of 0.625. For smaller aspect ratios the constant increases. At an aspect ratio of 2, the value os 0.7. The rotor disk has a circular plan form with an aspect ratio of $4/\pi$. No data is available for the constant of proportionality for this aspect ratio, but it is assumed that the constant has a value of at least 0.7. Thus approximately

$$v_i \simeq .7\ C_L\ V \tag{5}$$

Combining equations (4) and (5) yields a relationship for the maximum induced velocity of the rotor trailing vortex system.

$$v_i = \frac{1.4\ C_T\ V_T}{\mu} \tag{6}$$

Where $V_T$ is the tip speed, and $C_T$ is the rotor thrust coefficient defined as;

$$C_T = \frac{T}{\rho \pi R^2 V_T{}^2} \tag{7}$$

$\mu$ is the tip speed ratio given by:

$$\mu = \frac{V}{V_T} \tag{8}$$

with equations (2), (3), and (6), an expression for the core radius can be found.

$$a = \frac{k}{1.4\pi} R \tag{9}$$

Thus by comparing the rotor to an equivalent fixed wing, an estimate can be obtained for the core size of the rotor's trailing vortices. An alternate method will now be presented for accomplishing the same thing.

Detailed Examination of the Rotor Vortex System

A rotor in forward flight generates a bound circulation on the rotor blades which varies both radially and azimuthally. This leads to the supposition that the trailing vortices from each side of the rotor are not of equal strength. If true, a more accurate measure of the circulatory strength is necessary.

A rotor sheds a trailing vortex from each rotor blade tip. For moderate tip speed ratios these tip vortices can combine downstream from the rotor to form two trailing vortices as noted earlier. If the strength of one of the combined trailing vortices is denoted as $\Gamma_\infty$, then an amplification factor, $A_f$, will be defined as the ratio of $\Gamma_\infty$ to the product of the number of blades and the strength of the rolled-up tip vortex produced by one blade.

$$A_f = \frac{\Gamma_\infty}{B\Gamma_B} \tag{10}$$

Denoting the quantity $B\Gamma_B$ as $\Gamma_o$, the total strength for B blades, equation (10) is simply:

$$A_f = \frac{\Gamma_\infty}{\Gamma_o} \tag{11}$$

An approximate estimate of the amplification factor can be made solely on the basis of the geometry of the rotor tip path. First, it is assumed that the vortex from any single blade is coincident with the blade's tip path. Now, for a rotor system traveling in the negative x direction with velocity V, the equations describing the tip path coordinates are,

$$x = R \cos (\phi + \omega t) - Vt \tag{12}$$

$$y = R \sin (\phi + \omega t) \tag{13}$$

where $\phi$ is the angle defining the rotor blade position at time $t = 0$, $\omega$ is the angular velocity of the rotor, and R is the rotor radius. Figure 4 is a plot of the tip path of one rotor blade. If the coordinate system origin corresponds to time $t = 0$, then negative time denotes a positive x coordinate. The substitution $\psi = -\omega t$ is made in equations (12) and (13). Non-dimensionalizing by the rotor radius yields,

$$x/R = \cos (\phi - \psi) + \mu\psi \tag{14}$$

$$y/R = \sin (\phi - \psi) \tag{15}$$

For any x station there can be from one to an infinite number of $\psi$ values which satisfy equation (14), depending on the value of the other parameters. Each solution represents a separate vortex filament located at that particular x station. If each trailing vortex is comprised of one half of the filaments located at any x station which combine to form that vortex, then an estimate of the amplification factor would be one half of the number of solutions for $\psi$ in equation (14). Because equation (14) is a transcendental equation a general solution is difficult to obtain. An approximate solution can be made, however. We begin by rearranging equation (14) as,

$$x/R - \mu\psi = \cos (\phi - \psi) \tag{16}$$

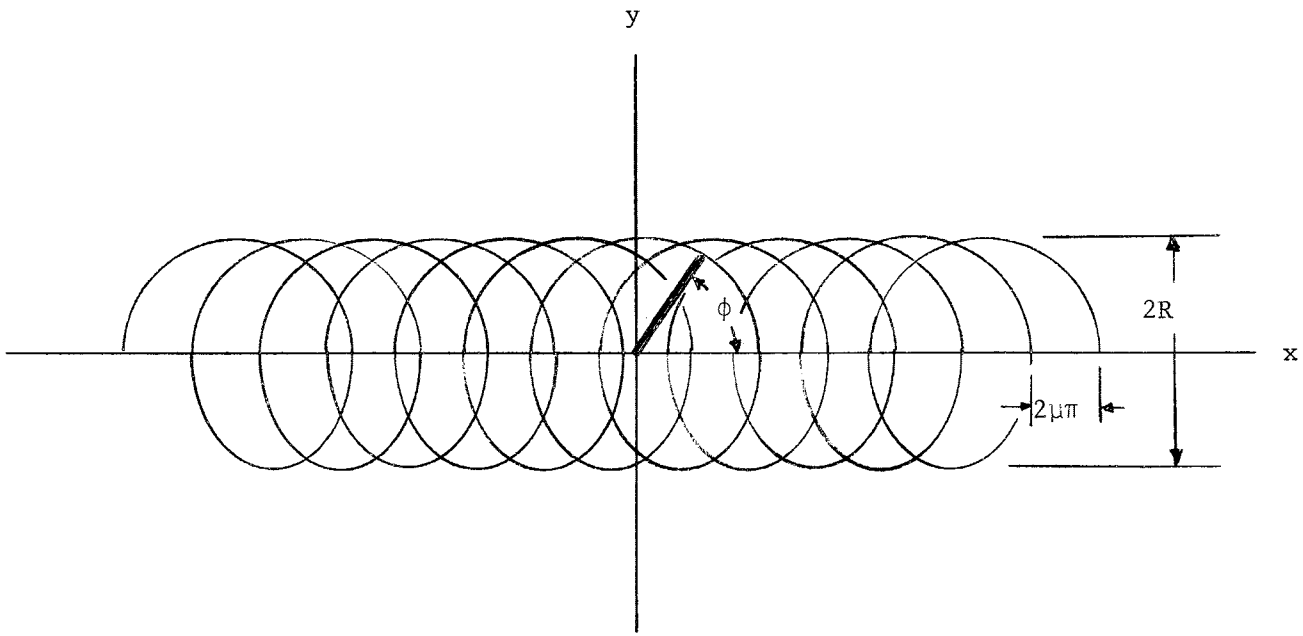


Figure 4. Typical Rotor Blade Tip Path (Equations 14 and 15).

Plotting both sides of equation (16) separately, and superimposing them on the same plot, results in Figure 5. It is evident that all of the solutions to equation (16) will occur within the region defined by $|x/R - \mu\psi| \leq 1$. The length of this region is then

$$\Delta\psi = 2/\mu \tag{17}$$

If the tip speed ratio is sufficiently small, the number of intersections of the cosine function with the $\psi$ axis and the number of solutions to equation (16) will be approximately equal. The amplification factor is half the number of solutions, therefore,

$$A_f \simeq 1/\pi\mu \tag{18}$$

The important behavior to note from this simple analysis is that the amplification factor varies inversely with tip speed ratio. A more accurate estimate of the constant of proportionality will be made later. This approach also fails to consider the possibility of unequal strengths for the two trailing vortices. A more sophisticated approach is necessary.

Figure 6 is a sketch of the tip vortices from a 2-bladed rotor for three separate tip speed ratios. As the tip speed ratio increases it is evident that the advancing side has a greater number of filaments that can combine to form a trailing vortex. Eisenhuth and McCormick[14] noted that when two vortex filaments intersected each other there was a tendency for the filaments to combine into separate loops.

Figure 7 is an illustration of this behavior for the rotor vortex geometry of Figure 6. This figure further illustrates the uneven distribution of filaments as noted above. As the tip speed ratio increases the advancing side gains a greater portion of the shed tip vortices. This indicates that the advancing side of the rotor would

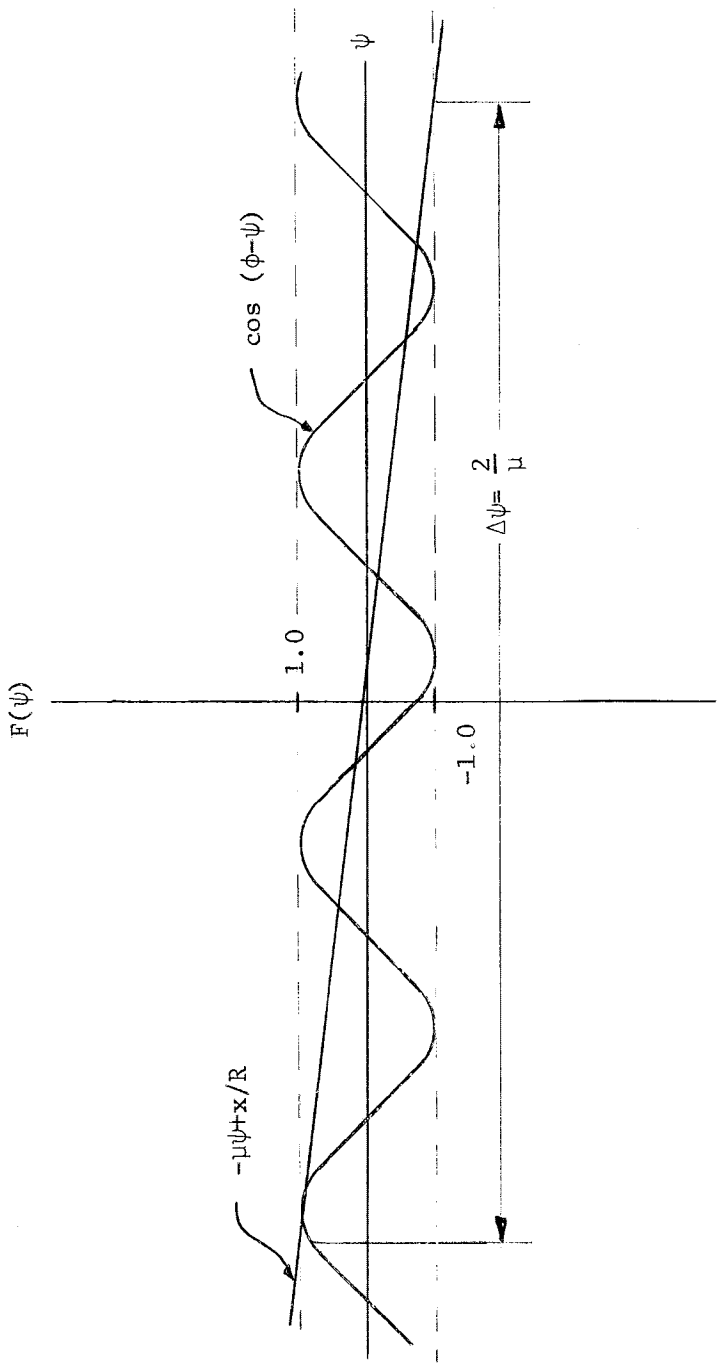


Figure 5. Equation 16.

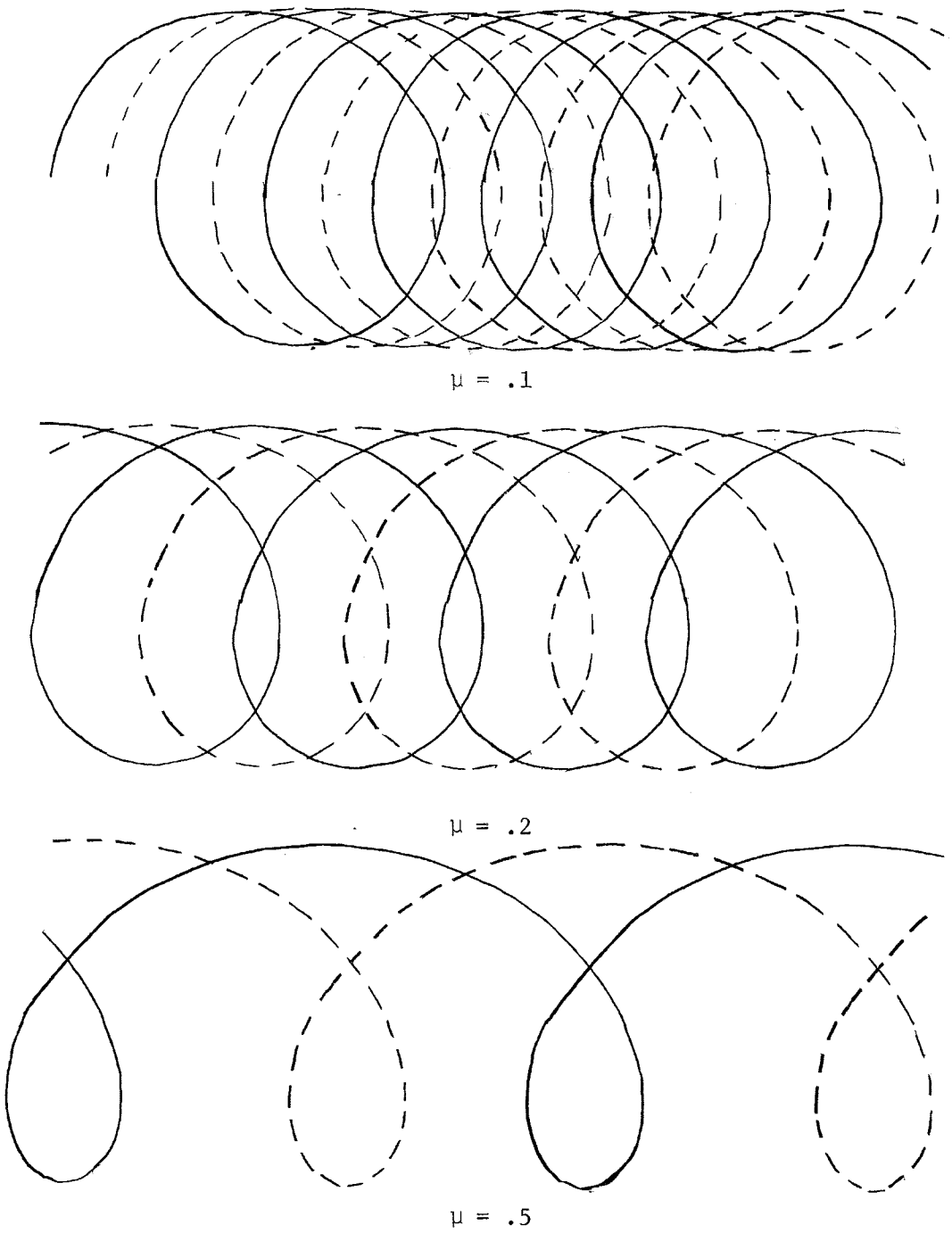


Figure 6. Tip Vortices for a Two Bladed Rotor at Three Different Tip Speed Ratios.

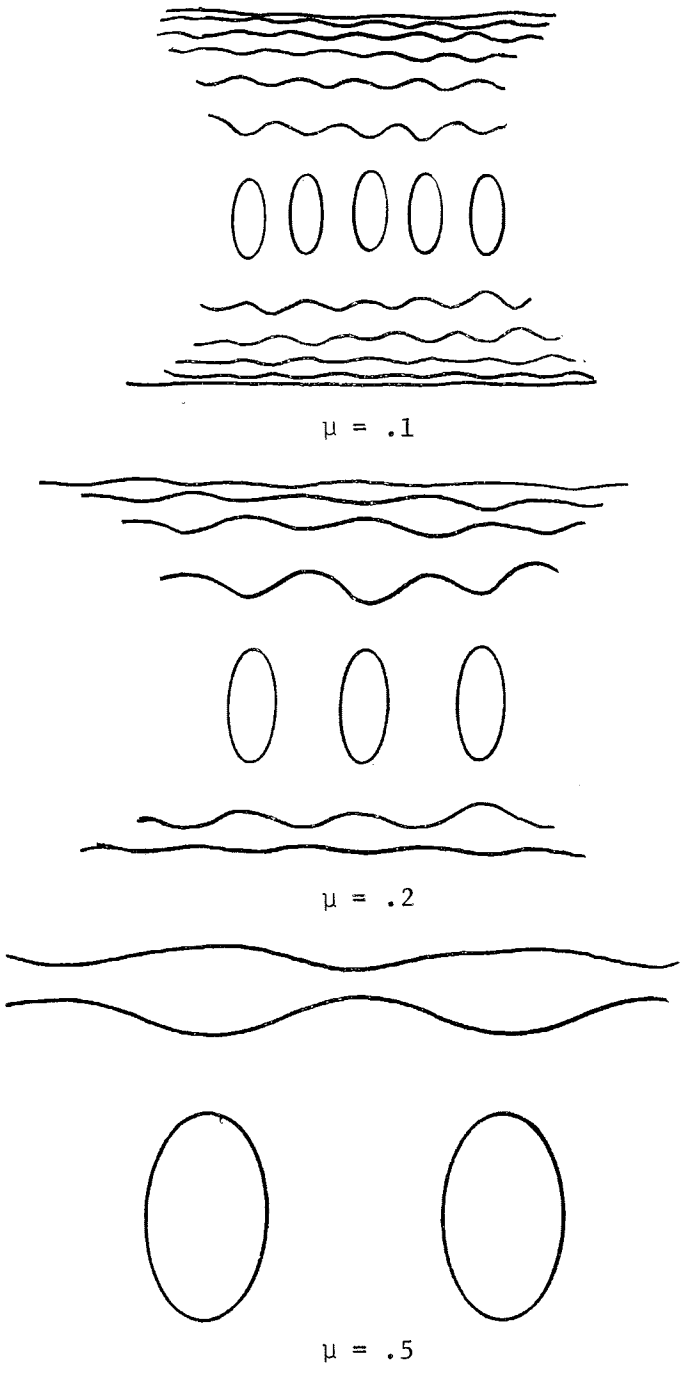


Figure 7. Tip Vortices of Figure 6 Combined into Separate Filaments.

have the stronger trailing vortex strength if the tip vortices are of constant strength. Thus, as the tip speed ratio increases equation (18) may become progressively inaccurate, since it is based on assuming that the two trailing vortices are of equal strength.

Flapping Rotor in Forward Flight

A more accurate estimate for the amplification factor can be made using the relationships derived for a flapping rotor without taper or twist by Gessow and Myers[15]. The lift per blade integrated over one period of revolution is:

$$L \simeq \frac{1}{6} \rho a_o \theta_o c R \, V_T^2 \left[1 + \frac{3}{2} \mu^2 + \frac{3}{2} \frac{\lambda}{\theta_o}\right] \tag{19}$$

where $\lambda$ is defined as the inflow ratio, $\theta_o$ is the hub pitch angle, and $a_o$ is the slope of the lift curve of the rotor airfoil section. The bound circulation on any rotor blade is found to be:

$$\Gamma(x,\psi) = \frac{1}{2} c a_o \theta_o V_T \left[x + \frac{\lambda}{\theta_o} + \frac{1}{2} \mu \frac{a_1}{\theta_o} + \sin\psi\left(\mu - \frac{a_1}{\theta_o} x\right) - \cos\psi \left(\mu \frac{\beta_o}{\theta_o} + x \frac{b_1}{\theta_o}\right)\right] \tag{20}$$

where $\beta_o$, $a_1$, $b_1$, are respectively the coning angle, longitudinal flapping and lateral flapping. Integrating over one period of revolution to find the mean bound circulation at any station on the blade yields:

$$\bar{\Gamma}(x) = \frac{1}{2\pi} \int_0^{2\pi} \Gamma(x,\psi)\, d\psi = \frac{1}{2} c a_o \theta_o V_T \left[1 + \frac{\lambda}{\theta_o} + \frac{1}{2} \frac{a_1}{\theta_o}\right] \tag{21}$$

From a moment balance on the rotor blade the longitudinal flapping coefficient is:

$$a_o = \frac{\mu}{1-1/2\mu^2}\left(\frac{8}{3}\theta_o + 2\lambda\right) \tag{22}$$

Assuming that the maximum bound circulation occurs at the tip of each rotor blade, then each shed tip vortex has a mean circulation of

$$\Gamma_B = \frac{1}{2}ca_o\theta_o V_T\left[1+\frac{\lambda}{\theta_o}+\frac{1}{2}\frac{a_1}{\theta_o}\right] \tag{23}$$

Combining equations (19) and (23) yields:

$$L = \frac{1}{3}\rho R V_T \Gamma_B \quad \frac{1+\frac{3}{2}\mu^2+\frac{3}{2}\frac{\lambda}{\theta_o}}{1+\frac{\lambda}{\theta_o}+\frac{1}{2}\mu\frac{a_1}{\theta_o}} \tag{24}$$

for the resultant lift per cycle per blade. For B blades the rotor lift then becomes:

$$L = \frac{1}{3}\rho R V_T \Gamma_o \quad \frac{1+\frac{3}{2}\mu^2+\frac{3}{2}\frac{\lambda}{\theta_o}}{1+\frac{\lambda}{\theta_o}+\frac{1}{2}\mu\frac{a_1}{\theta_o}} \tag{25}$$

The lift for a wing of semi-span R and flight speed V with an elliptical circulation distribution is,

$$L = \frac{\pi}{2}\rho V R \Gamma_\infty \tag{26}$$

where $\Gamma_\infty$ is the mid-span circulation of the wing. The ratio of $\Gamma_\infty$ to $\Gamma_o$, i.e. the amplification factor, is then,

$$A_f = \frac{2}{3\pi\mu} \quad \frac{1+\frac{3}{2}\mu^2+\frac{3}{2}\frac{\lambda}{\theta_o}}{1+\frac{\lambda}{\theta_o}+\frac{1}{2}\mu\frac{a_1}{\theta_o}} \tag{27}$$

Equation (27) is plotted in Figure 8 versus tip speed ratio for various $\lambda/\theta_o$'s. For a model described in Reference 16, $\lambda/\theta_o$ was found to be

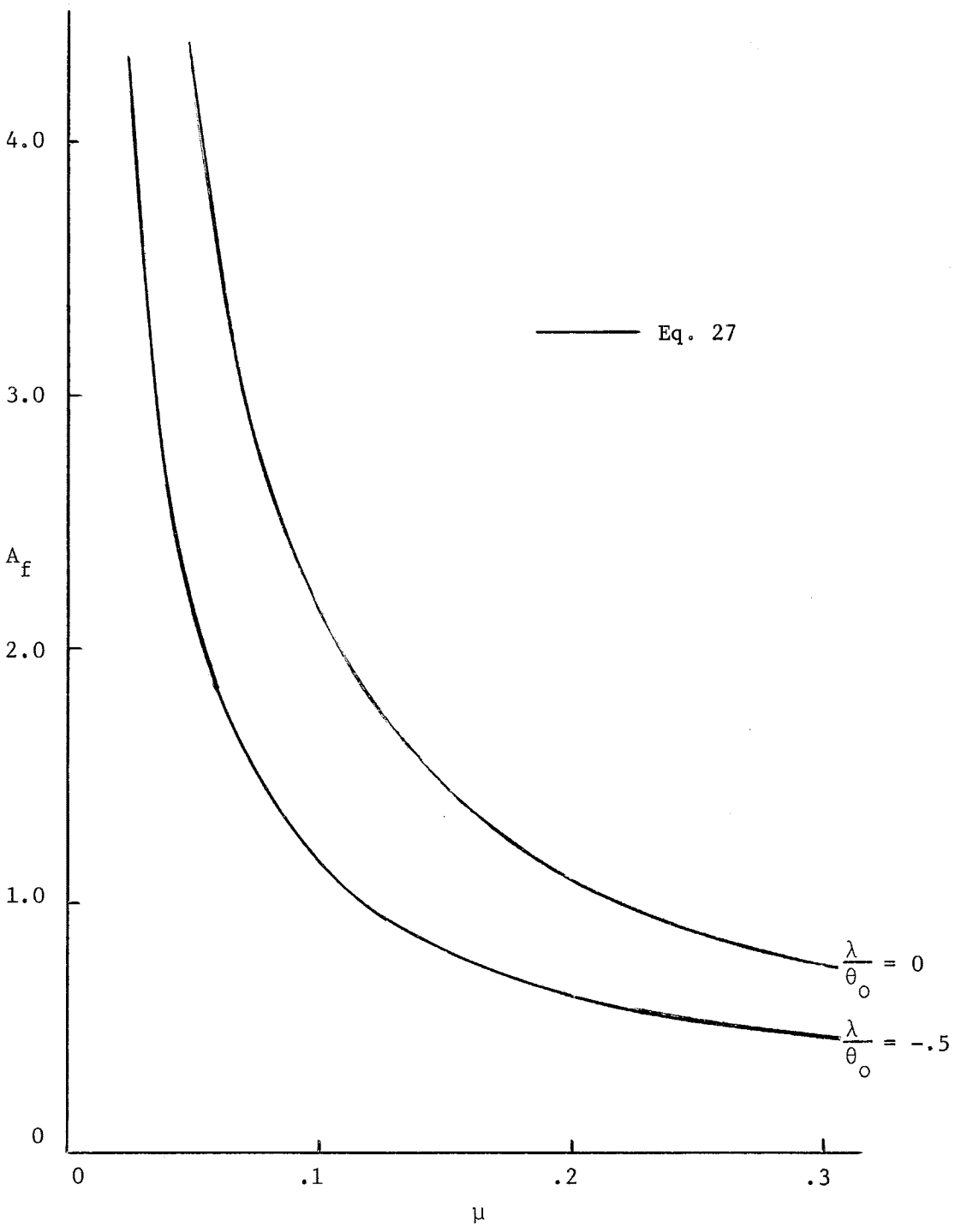


Figure 8. Amplification Factor vs. Tip Speed Ratio.

approximately -.152 for a tip speed ratio of .31. From Figure 8 it can be seen that for this case the amplification factor behaves essentially as:

$$A_f = \frac{2}{3\pi\mu} \tag{28}$$

with some slight change in magnitude. It should be noted here that the variables involved in equation (27) are interdependent and must therefore be determined for a given flight condition to obtain an accurate estimation of the amplification factor. For a first estimate the term in the brackets of equation (27) can probably be assumed equal to unity.

Equation (27) is still based on the assumption that the two trailing vortices for the rotor system have equal strengths. This assumption is reasonable because a trimmed rotor must behave in the same manner as a fixed wing; the induced downwash should be symmetrical about the $\psi = 0, 180^{o}$ line. This occurs when the trailing vortices have equal strengths. But, Figure 7 indicates that this is not true if one assumes a mean circulation strength for the tip vortices as is done to obtain equation (27). The following analysis will show why the trailing vortices do have approximately equal strengths.

The tip circulation from equation (20) is:

$$\Gamma_B(\psi) = \frac{1}{2} ca_o \theta_o V_T [\Gamma_1 + \Gamma_2 \cos\psi + \Gamma_3 \sin\psi] \tag{29}$$

where $\Gamma_1$, $\Gamma_2$, and $\Gamma_3$, can be found from equation (20). It is assumed that this is also the maximum bound circulation and therefore the tip vortex circulation. From a moment balance of the rotor in Reference 15, the lateral flapping coefficient $b_1$ is

$$b_1 = \frac{4\mu\beta_o}{3(1+\frac{1}{2}\mu^2)} \tag{30}$$

From equation (22) and (30) $\Gamma_1$, $\Gamma_2$, and $\Gamma_3$, become

$$\Gamma_1 = [1 + \frac{5}{6}\mu^2 + \frac{\lambda}{\theta_o}(1 + \frac{1}{2}\mu^2)]/(1 - \frac{1}{2}\mu^2) \tag{31}$$

$$\Gamma_2 = -\frac{\mu}{3}\frac{\beta_o}{\theta_o}\left(\frac{7 + \frac{3}{2}\mu^2}{1 + \frac{1}{2}\mu^2}\right) \tag{32}$$

$$\Gamma_3 = -\mu\left(\frac{5}{3} + \frac{1}{2}\mu^2 - \frac{2\lambda}{\theta_o}\right)/(1 - \frac{1}{2}\mu^2) \tag{33}$$

Equation (29) can be rewritten as:

$$\Gamma^* = \frac{\Gamma_B(\psi)}{\frac{1}{2}ca_o\theta_o V_T \Gamma_1} = 1 + \frac{\Gamma_2}{\Gamma_1}\cos\psi + \frac{\Gamma_3}{\Gamma_1}\sin\psi \tag{34}$$

From equations (31), (32), (33), and (34), it is apparent that as the tip speed ratio increases the advancing side's circulation decreases while the retreating side's circulation increases. On the other hand, Figure 7 shows that the number of vortices on the advancing side increases with $\mu$ while the number on the retreating side decreases. Thus Figure 7 leads to the conclusion that the two trailing vortices of the rotor system could have nearly equal strengths and that the amplification factor as defined by equation (27) will be valid.

To evaluate the constants on the sine and cosine functions of equation (34), the inflow ratio and coning angle must be known. The coning angle can be found from the following equation obtained by Gessow and Myers[15] from trim considerations.

$$\beta_o = \frac{\frac{1}{2}c\rho a_o\theta_o}{I_1}\left(\frac{3\lambda}{\theta_o} + \frac{1}{4}(1 + \mu^2) - \frac{M_w}{I_1\omega^2}\right) \tag{35}$$

where $I_1$ is the blade moment of inertia, $M_w$ the weight moment of the blade, and $\omega$ is the angular velocity of the rotor blade. The inflow ratio can be found from the following expression:

$$\alpha = \frac{\lambda}{\mu} + \frac{\frac{1}{2} C_T}{\mu(\mu^2 + \lambda^2)^{\frac{1}{2}}} \tag{36}$$

where $\alpha$ is the angle of attack of the rotor disk plane. The thrust coefficient is simply,

$$C_T = \frac{1}{2} a_o \sigma \theta_o \left[\frac{1}{3} + \frac{1}{2} \mu^2 + \frac{1}{2} \frac{\lambda}{\theta_o}\right] \tag{37}$$

where $\sigma$ is the rotor solidity.

$$\sigma = \frac{BL}{\pi R} \tag{38}$$

The longitudinal flapping coefficient can also be found from helicopter trim considerations[16]

$$a_1 + \alpha = \frac{-D}{W} \tag{39}$$

Equations (22), (36), (37), and (39), define a system of equations of five unknowns; $C_T$, $\alpha$, $a_1$, $\lambda$, $\theta_o$. Given the helicopter geometry, tip speed, flight speed, body weight, and drag characteristics, and a desired thrust coefficient, the above set of equations can be solved for the unknown quantities. Once these are known, the coning angle and lateral flapping coefficient can also be found.

Figure 9 is a plot of equation (34) for a fictitious helicopter operating at two different tip speed ratios. The helicopter characteristics are assumed to be:

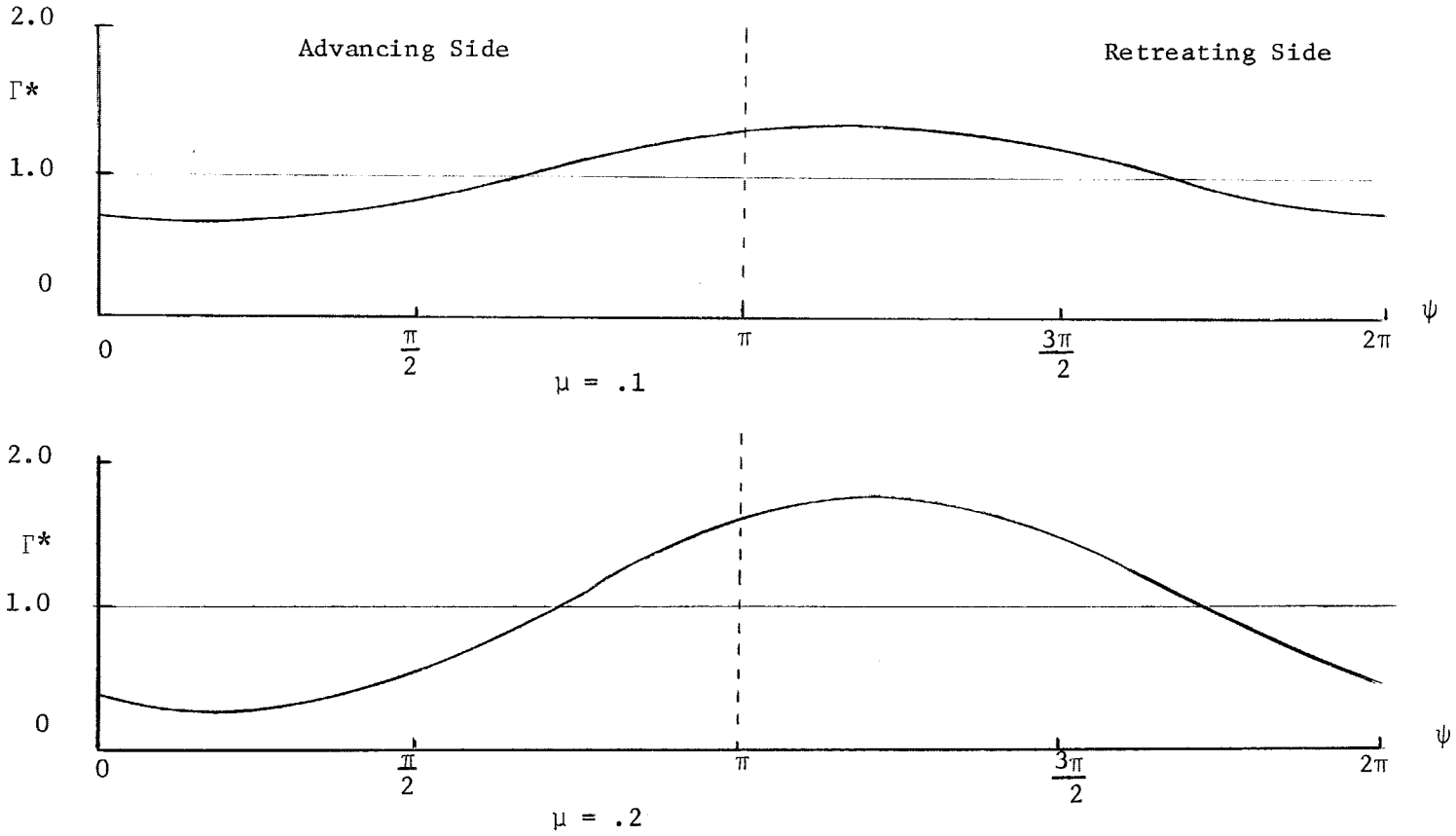


Figure 9. Non-dimensional Tip Vortex Circulation for Two Different Tip Speed Ratios (Eq. (34)).

$W = 7000$ lbs.

$V_T = 650$ fps

$\rho = .00237$ slug/ft$^3$

$\sigma = .06$

$a_o = 5.73$ C /rad

$f = 16$ ft$^2$ (equivalent flat plate area)

$C_T = .00555$

$R = 20$ ft.

$\mu = .1; .2$

$$\frac{M_w}{I_1 \omega^2} \cong .00228$$

$$\gamma = \frac{c\rho a_o R^4}{2I_1} \cong 5.5$$

This figure clearly illustrates that the tip vortices shed from each blade are stronger on the retreating side than those on the advancing side and that the difference becomes greater as the tip speed ratio increases.

Calculation of the Far Field Velocity Using a Potential Model

To see how accurately equation (28) models the amplification factor, a simple potential model of a helicopter wake is used to calculate the velocity field. This calculated velocity field can then be compared to a fixed wing velocity field to calculate the theoretical amplification factor.

For simplicity in calculating the rotor far field velocities it is assumed that the tip vortex from each blade is coincident with the tip

path for all time, rather than using a free wake analysis. The major difference between the two models is the relative location of the rotor wakes in the vertical direction. This fixed wake method allows a considerable savings in computer time for calculations of the far field velocity of the rotor vortex systems.

For the fixed wake model the Biot-Savart Law can be used to find the velocity at any point in the x-y plane. The relationship is

$$d\tilde{v} = \frac{\Gamma}{4\pi R} \frac{\tilde{p} \times d\tilde{s}}{|\tilde{p}|^3} \tag{40}$$

where $\tilde{p}$ and $\tilde{s}$ are non-dimensional vectors based on the rotor radius. For this model $\tilde{p}$ is the vector from the point of interest to any point of the vortex filament, and $d\tilde{s}$ is the differential length of the vortex filament at that point. Therefore,

$$\tilde{p} = (x - x_o)\,\tilde{i} + (y - y_o)\,\tilde{j} \tag{41}$$

and

$$d\tilde{s} = d\,x\,\tilde{i} + dy\,\tilde{j} \tag{42}$$

where x and y are defined by equations (14) and (15) respectively and have been non-dimensionalized by the rotor radius. Using the Biot-Savart Law for a system where the limits on $\psi$ are infinite, the velocity at any point in the x-y plane becomes:

$$v_i(x_o,y_o) = \frac{-\tilde{k}}{4\pi R} \int_{-\infty}^{\infty} \frac{\Gamma(\psi)\{(x-x_o)\cos(\phi-\psi)+(y-y_o)(\sin(\phi-\psi)+\mu)\}}{\{(x-x_o)^2 + (y-y_o)^2\}^{3/2}}\, d\psi \tag{43}$$

For simplicity we assume that the circulation strength differs only slightly from the mean value. From equation (34) it was shown that this assumption increases in error as the tip speed ratio increases, but for

a first approximation it is assumed to be sufficiently accurate. Using a constant circulation in equation (43) results in the following expression for the non-dimensional induced velocity.

$$\frac{4\pi R}{\Gamma} v_i(x_o,y_o) = -\bar{k} \int_{-\infty}^{\infty} \frac{\{(x-x_o)\cos(\phi-\psi)+(y-y_o)(\sin(\phi-\psi)+\mu)\}}{\{(x-x_o)^2+(y-y_o)^2\}^{3/2}} d\psi \tag{44}$$

The limits of integration have been taken over all $\psi$ because this model is used to obtain the amplification factor in the ultimate wake. This equation was evaluated by numerical integration.

A wing in forward flight generates a vortex sheet which rolls up into two vortices which lie inboard from the wing tips. The far field velocities can be calculated by assuming that the tip vortices are two discreet vortex filaments starting at the wing tips and continuing to infinity. However the inboard movement of the trailing vortices will be ignored in this analysis since it is assumed that the rotor-generated far field vortices also have no inboard movement.

The Biot-Savart Law for a straight line filament of finite length reduces to

$$v(h) = \frac{\Gamma}{4\pi h}(\cos\gamma + \cos\beta) \tag{45}$$

where $\gamma$, $\beta$, and h are defined in Figure 10. For a wing semi-span of R centered in the x-y plane origin, the far field velocity can be found by the use of equation (45) applied to the two filament system. For this trailing vortex system defined in the x-y plane, the non-dimensional induced velocity in the z direction becomes:

$$\frac{4\pi R}{\Gamma} v(y_o) = \frac{4}{y_o^2-1} \tag{46}$$

where $y_o$ has been non-dimensionalized by the semi-span.

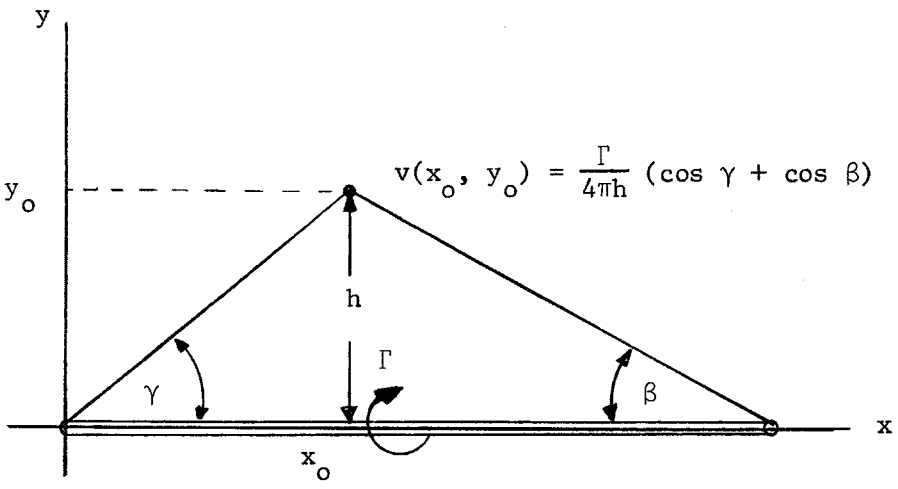


Figure 10. Biot-Savart Law as Applied to the Geometry of a Finite Length Vortex Filament.

As stated previously the analytical model presented here is based on a fixed-wake geometry. Because of this the velocity field at any x station is highly dependent on the blade position at time t = 0. To overcome this dependency it is desirable to take results from various x stations defined over one region of periodicity. For each x station an amplification factor can be found when the rotor velocity field is compared to the equivalent fixed wing velocity field. This is done by calculating the necessary circulation of the wing such that the velocity fields described by equations (44) and (46) match. From these results amplification factors for each x station within one region of periodicity are calculated and then averaged to obtain a time averaged value.

The region of periodicity is found in the following manner. This region is the change in the downstream coordinate, x, as the rotor blade goes through one revolution. The period of one revolution is

$$T = \frac{2\pi}{\omega} \tag{47}$$

With the use of equation (14) the change in x is found to be:

$$\Delta x = 2\pi R\mu \tag{48}$$

This region can be broken into several small intervals as described above to evaluate the amplification factor.

Numerical integration of equation (44) was done on an IBM 360/67 digital computer. Since the limits of integration extend over all $\psi$ a finite integration angle must be used. A description of the truncation of $\psi$ is given in Appendix II. The resulting velocity fields were compared with the velocity described by equation (46) for a fixed wing, and an amplification factor was found. Figure 11 presents the predicted amplification factor as a function of tip speed ratio for a single

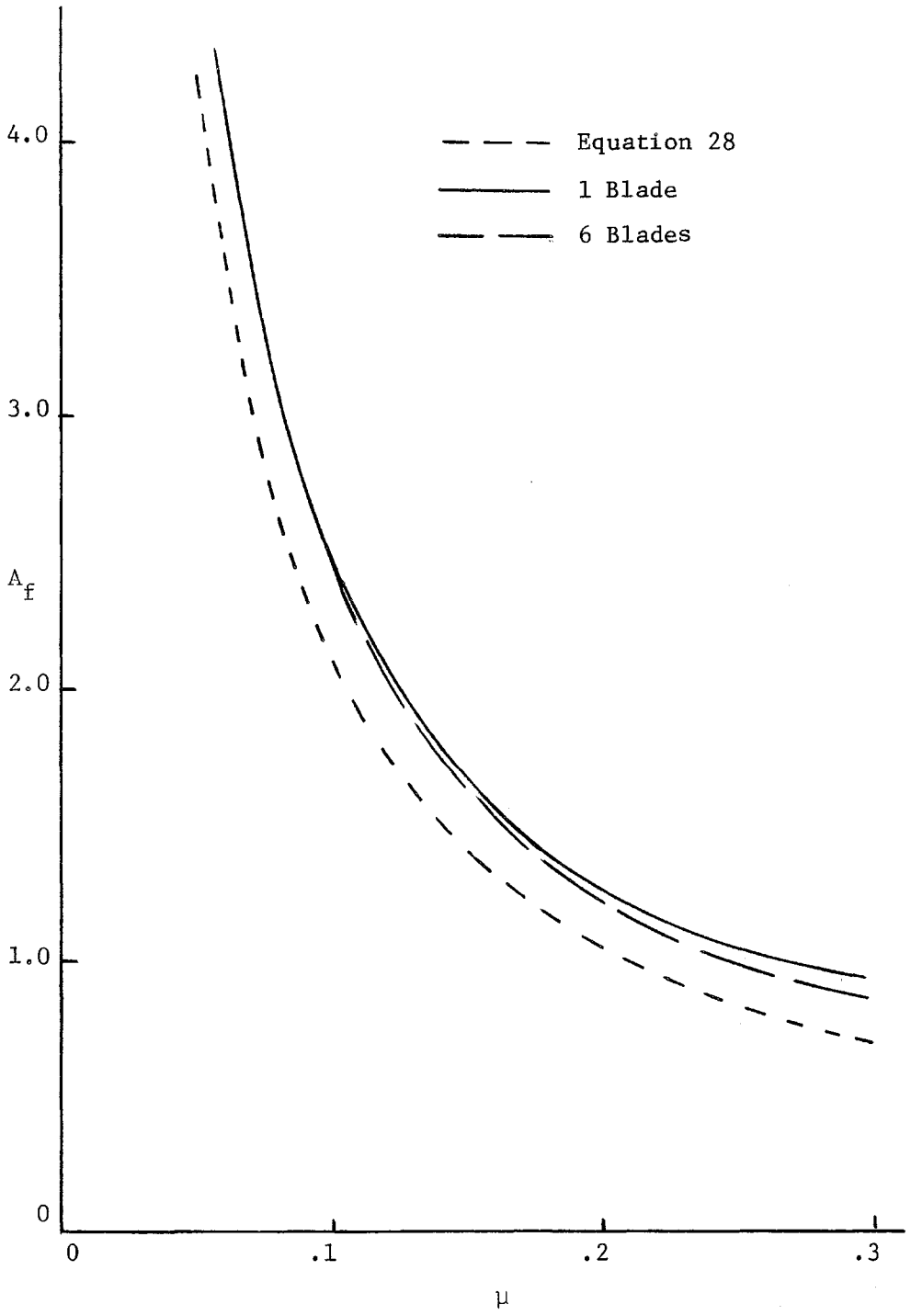


Figure 11. Amplification Factor vs. Tip Speed Ratio Calculated with Potential Model (5% cutoff error).

bladed rotor and a six bladed rotor. The amplification factor was found to be essentially independent of the number of rotor blades used and given by:

$$A_f \simeq \frac{.25}{\mu} \tag{49}$$

This agrees reasonably well with equation (28) and appears to justify the gross treatment of the rotor as an equivalent wing.

# CHAPTER III

# EXPERIMENTAL STUDY

## Description of Experimental Apparatus

The model used for the velocity field measurements was a two-bladed untwisted teetering rotor with a radius of 11" and a hub radius of 1.5". The rotor section was a NACA 0012 airfoil section with a chord of 2". The rotor hub was made of steel and the rotor blades of aluminum. The model rotor was dynamically balanced for rotational speeds of up to 1800 rpm, the maximum speed that the motor could turn the rotor. All measurements were taken with a hub pitch angle of 10 degrees. The rotor was driven by a variable speed 3/4 hp motor. The rotor was tested in the 4 x 5 foot subsonic wind tunnel at The Pennsylvania State University, Department of Aerospace Engineering. For all measurements the rotor disk plane was aligned with the free stream velocity such that the rotor disk had no angle of attack.

Three different tip speed ratios were tested. For each case the velocity measurements downstream from the rotor model were taken with a $45^{o}$ hot-wire probe mounted on a motor-driven traversing mechanism and used in conjunction with a battery operated anemometer. The signal is converted to a linearly proportional signal using King's Law. (See Appendix I). Figure 12 is a diagram of the analog circuitry used for the conversion. A EAI model TR-20 Analog Computer was used for this purpose. The signal is first filtered to remove high frequency information and then passed into the analog computer. The resulting signal is then sent into a EAI model 1130 Variplotter. The y-plot

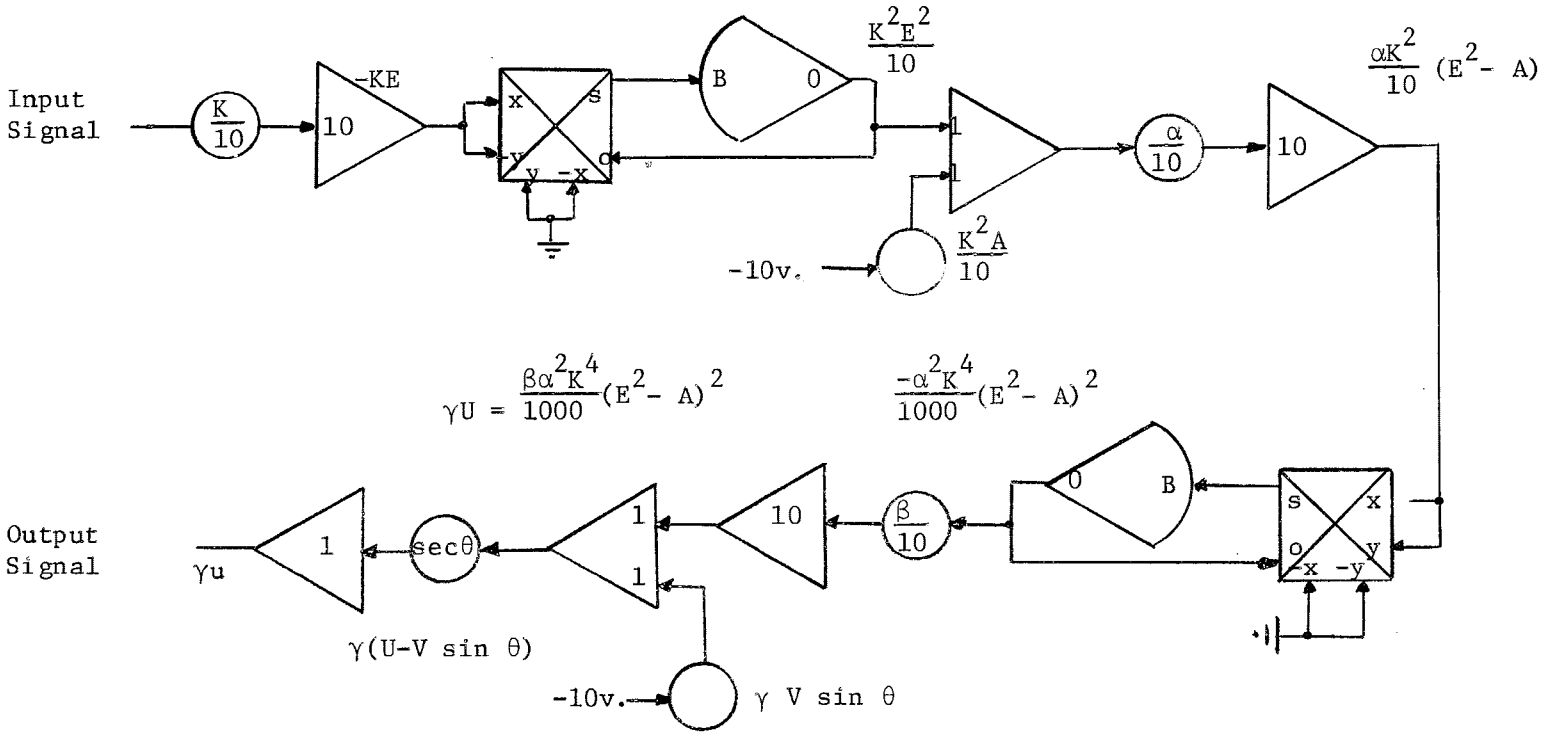


Figure 12. Analog Circuit Diagram for Converting Hot Wire Signal to a Linear Voltage Output, Using King's Law.

signal is driven by a voltage from a potentiometer mounted on the traversing mechanism and the velocity signal is recorded on the Variplotter. Figure 13 is a block diagram of the electronic equipment used in this set-up, and Figure 14 is a sketch of the experimental set-up.

Test of the Hot-Wire Anemometer

In order to test the validity of the hot-wire as a measuring device and to gain confidence in the hot-wire output as compared to known velocity fields measured with a vortex meter, the hot-wire was first used to measure the velocity field behind a fixed wing for three different operating conditions.

The wing used had a NACA 0015 section profile, a semi-span of 18", and a chord of 6". Figure 15 is a plot of the maximum measured induced tangential velocity versus the wing $C_L$. Good agreement with the results of McCormick et al.[2] was obtained for the maximum induced velocity. Figure 16 is a typical plot of the induced velocity field versus radial position for the measurements taken. The induced velocity has been non-dimensionalized by the free stream velocity. The core radius for this case was found to be approximately 0.47 inches. This gives a circulation at the core radius of 3.57 $ft^2/sec$. The estimated mid-span circulation for this core was 5.43 $ft^2/sec$. The value for k in equation 3 for this case was found to be 0.658. All measurements were taken 33" downstream of the rotor trailing edge. From these results it appears that the trailing vortices behave in the manner predicted by the Navier-Stokes solution as expressed in Reference 2. The results also indicated that the hot-wire would be a reliable measuring device.

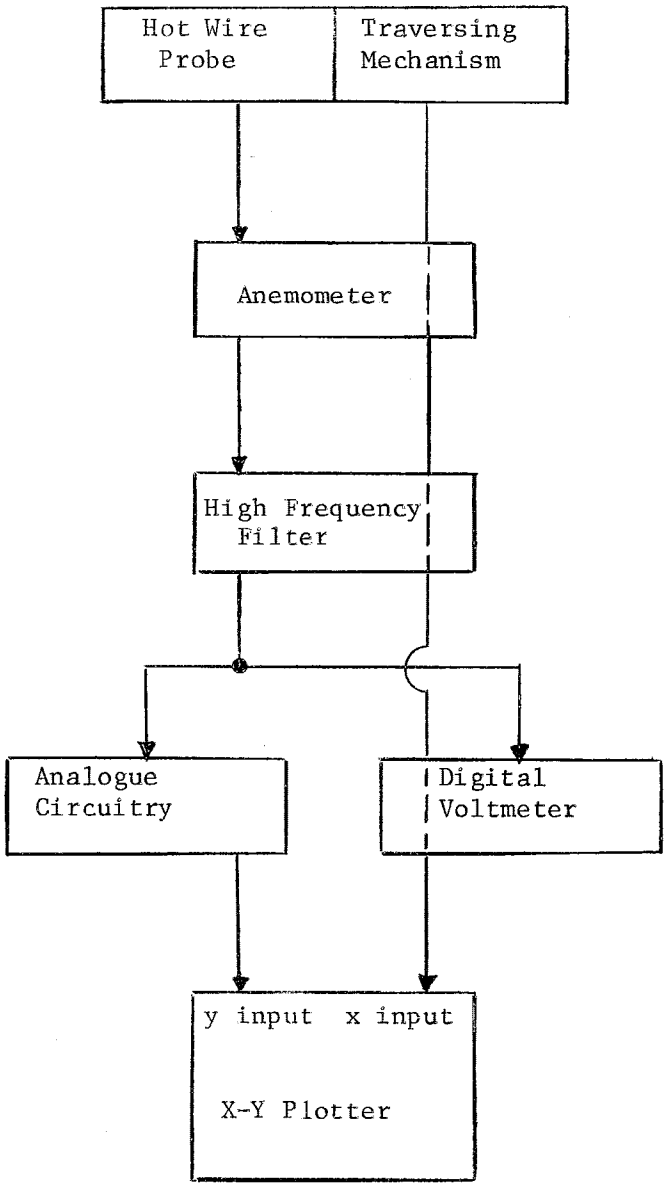


Figure 13. Data Collection and Recording System.

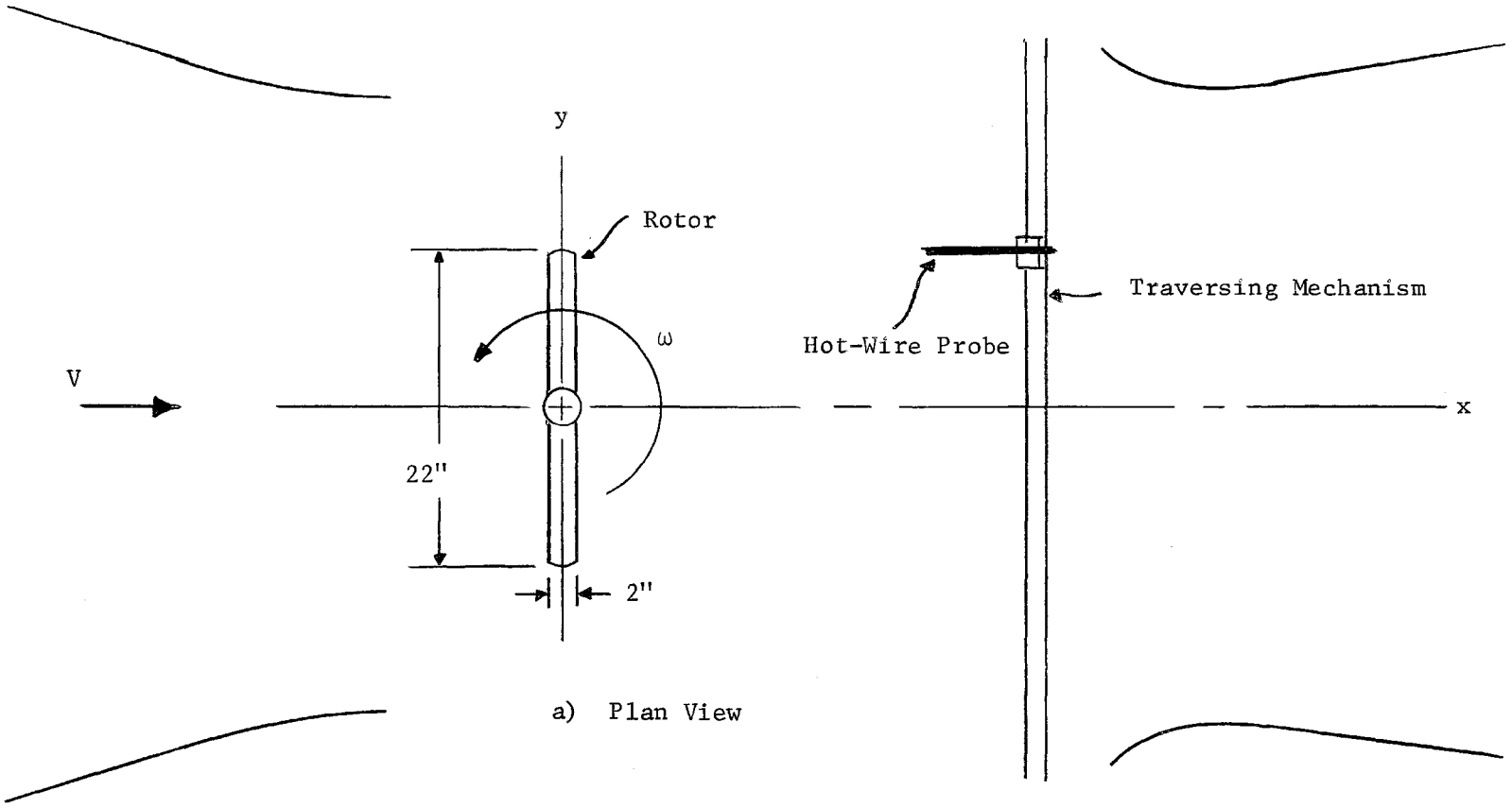


Figure 14. Schematic Diagram of Experimental Apparatus in Test Section.

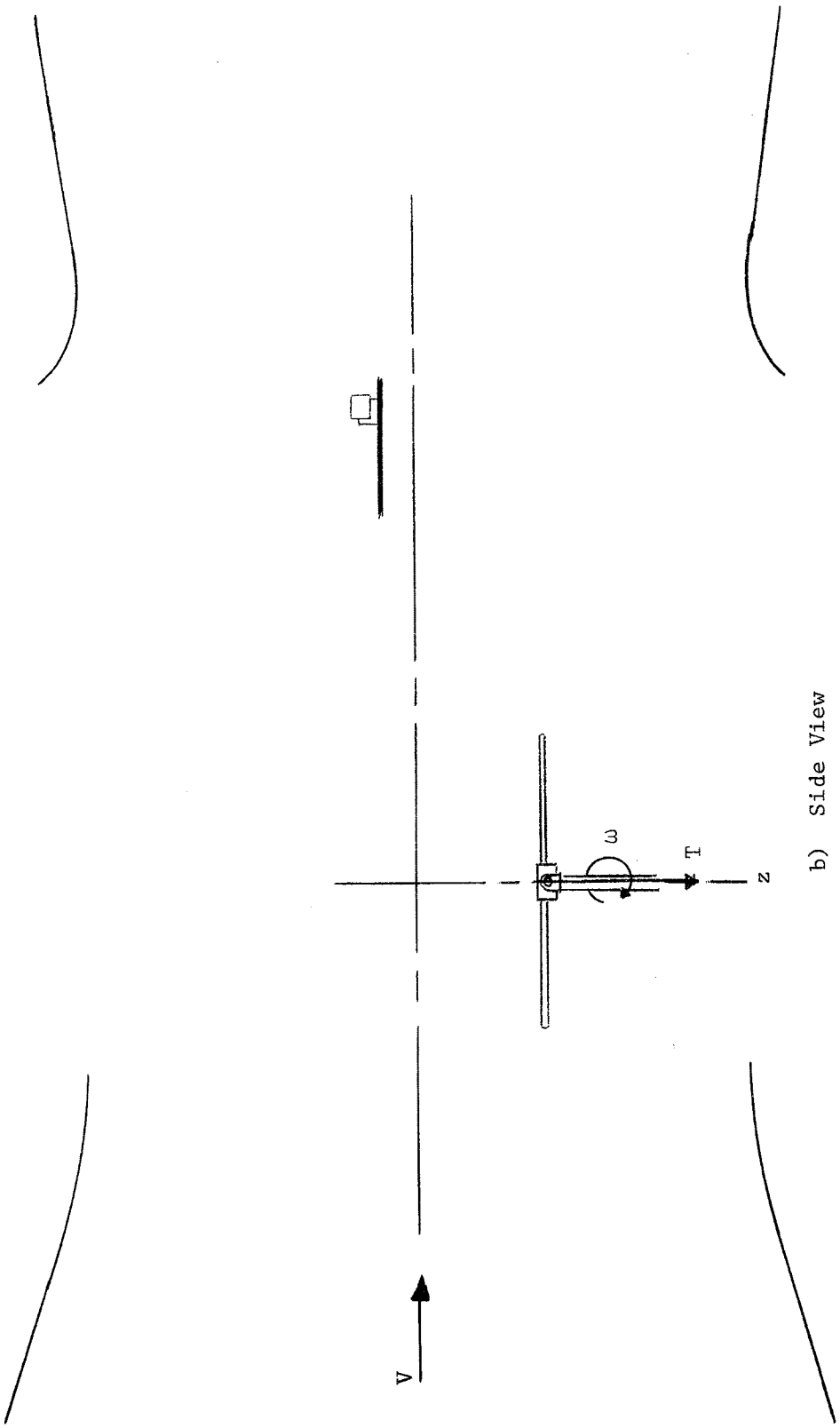


b) Side View

Figure 14. (Continued)

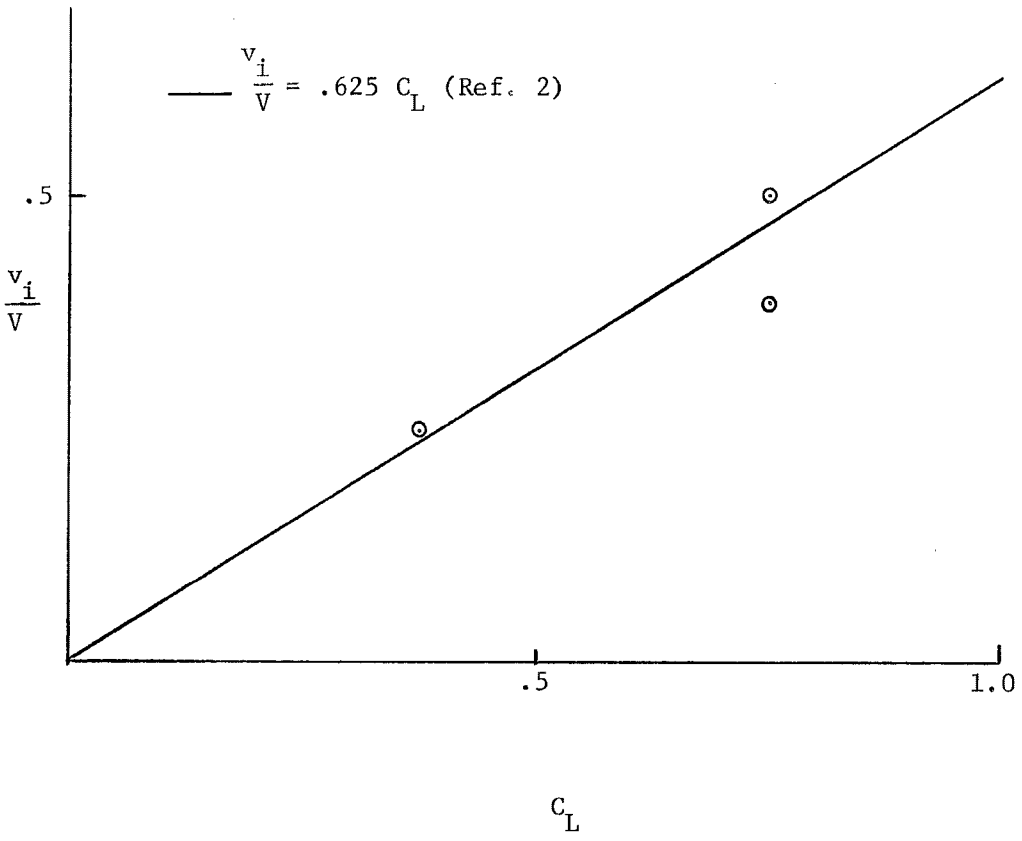


Figure 15. Measured Values of $\frac{v_i}{V}$ vs. $C_L$ for Fixed Wing.

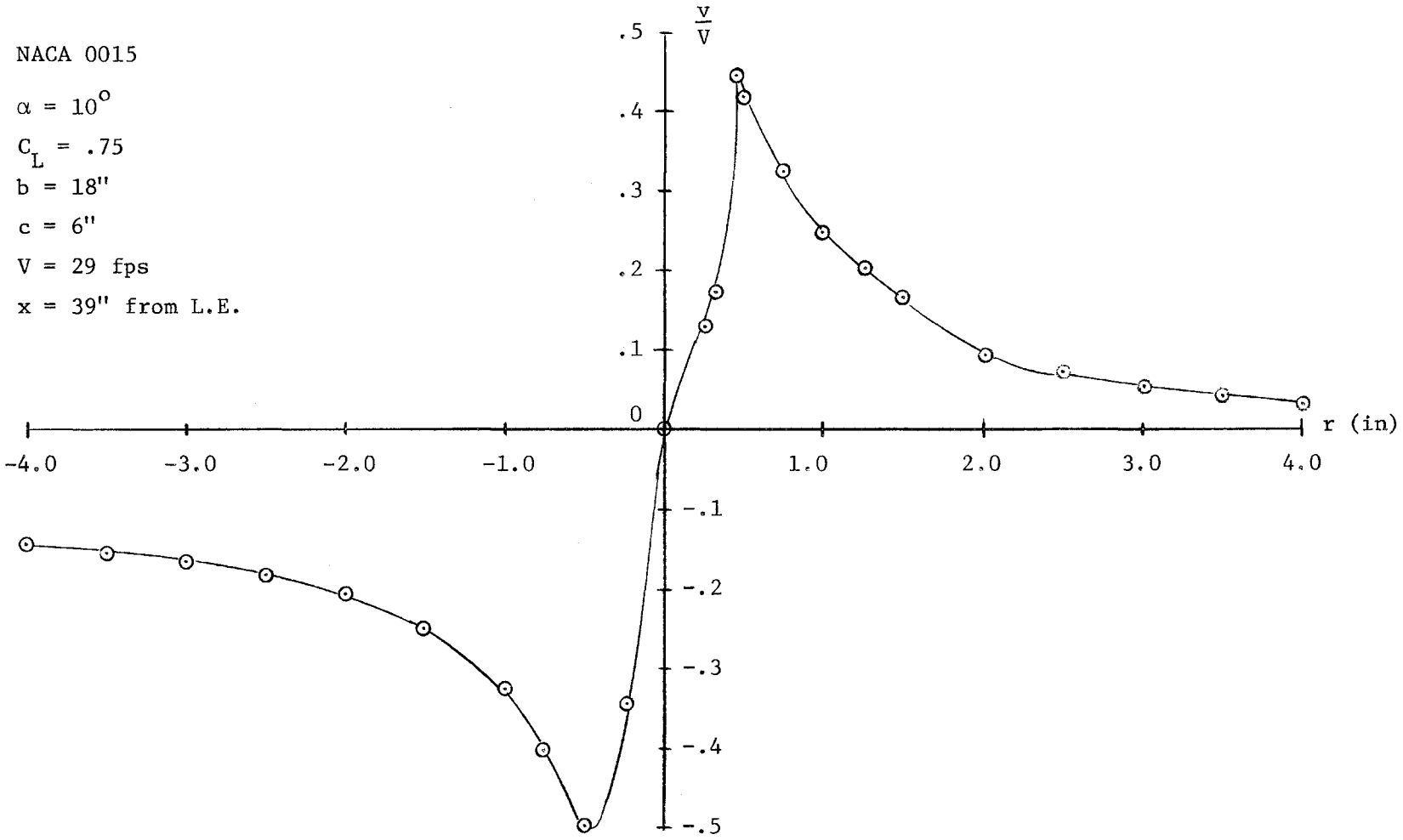


Figure 16. Tangential Velocity Field Measured Behind Fixed Wing Using a Hot Wire. (Core Centered)

Measurements of Rotor Velocity Field and Sample Calculations

Having gained confidence from the fixed wing tests, the hot-wire was then used to measure the velocity field behind the teetering rotor model as described previously. Three different operating conditions were measured. In each case the velocity field measured along the y-axis downstream of the rotor was recorded on the Variplotter. This was done at intervals of 1 inch in the z direction. All velocities were measured at x/R = 3.55. In this manner the vortex cores were located for both advancing and retreating sides. Because the single $45^{o}$ hot-wire probe is only calibrated for velocities in the plane defined by the intersection of the mean tunnel velocity and the wire itself, only calibrated signals are obtained when the probe passes through or close to the vortex core center. These core centered measurements are the measurements used in this study.

As noted earlier, the rotor disk plane was aligned with the free stream velocity. Lateral flapping was negligible for all cases studied. For a zero angle of attack of the rotor disk plane, the inflow ratio is

$$\lambda = \frac{-w}{V_T}$$

where w is the downwash of the rotor. Assuming a constant downwash equal to the mean downwash of the rotor in forward flight, and taking finite hub radius and tip losses into consideration, equation (37) becomes

$$C_T = \frac{1}{2}\sigma a_o \theta_o \frac{\frac{1}{3}(T_B^3 - h^3) + \frac{1}{2}\mu^2 (T_B - \mu)}{1 + \frac{T_B^2 - h^2}{8}\frac{a_o \sigma}{\mu}}$$

where $T_B$ has the value .97 and h is the hub radius non-dimensionalized by the rotor radius.

The far field circulation can then be found by the use of equation (2) rewritten in terms of the thrust coefficient and tip speed ratio.

$$\Gamma_\infty = 2C_T R \frac{V_T}{\mu}$$

The bound circulation at the tip is found from Equation (20). For this teetering rotor model it is:

$$\Gamma(\psi) = \frac{1}{2} ca_o \theta_o V_T [1 - \frac{C_T}{2\mu\theta_o} + \mu \sin \psi]$$

Table 1 is a listing of the operating parameters used for the three different cases studied, and the calculated parameters of interest. Sample calculations for one case are presented in Appendix III.

# CHAPTER IV

## RESULTS

Figure 17 is a typical example of the velocity profile measured by the hot-wire anemometer behind the rotor as it was plotted by the Variplotter for this study. Figure 18 is the same plot with the small scale oscillations faired out, and with velocity magnitude added. These measurements were taken at the z station representing the vortex center for which the core diameter and maximum tangential velocities were largest.

Because the measurements taken for this study were for a small scale model, Heyson's[11] measured velocities behind a large scale model were incorporated in this study to obtain more information concerning rotor far field velocities. Heyson's measurements were taken at various x, y, and z stations underneath and behind a rotor model. The rotor used was a teetering type with untapered, untwisted blades. The rotor blades had a NACA 0012 airfoil section. The rotor radius was 7.5 feet with a solidity of .0534. In order that Heyson's data correspond as accurately as possible to data taken in this study, the velocity measurements at the x/R station of 3.14 in Heyson's study were used, these measurements being the closest to the x/R station of 3.55 used in this project's study. All velocity measurements for Heyson's study were made with pitot tube rakes. Because of this, the velocity measurements are time averaged values. These measurements were made in the NASA Langley's full scale wind tunnel. For each case the measurements at the z station which had the greatest tangential

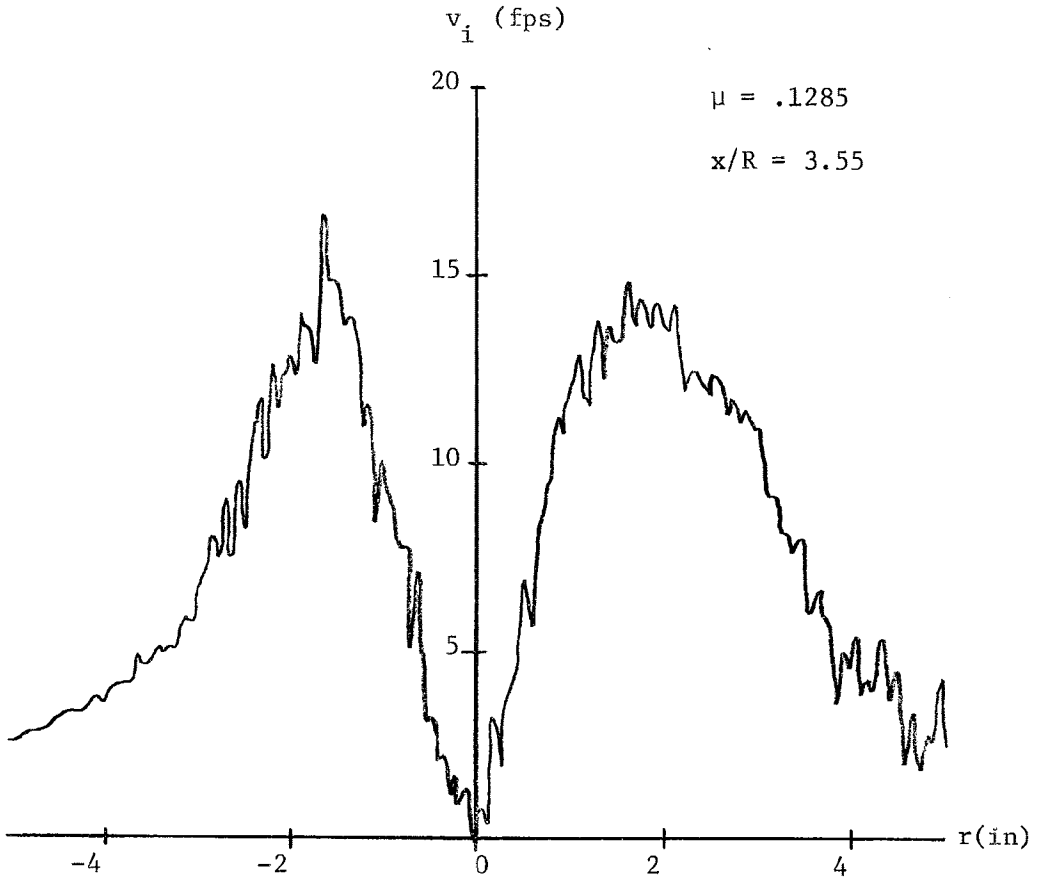


Figure 17. Typical Trace of Variplotter Output Signal.

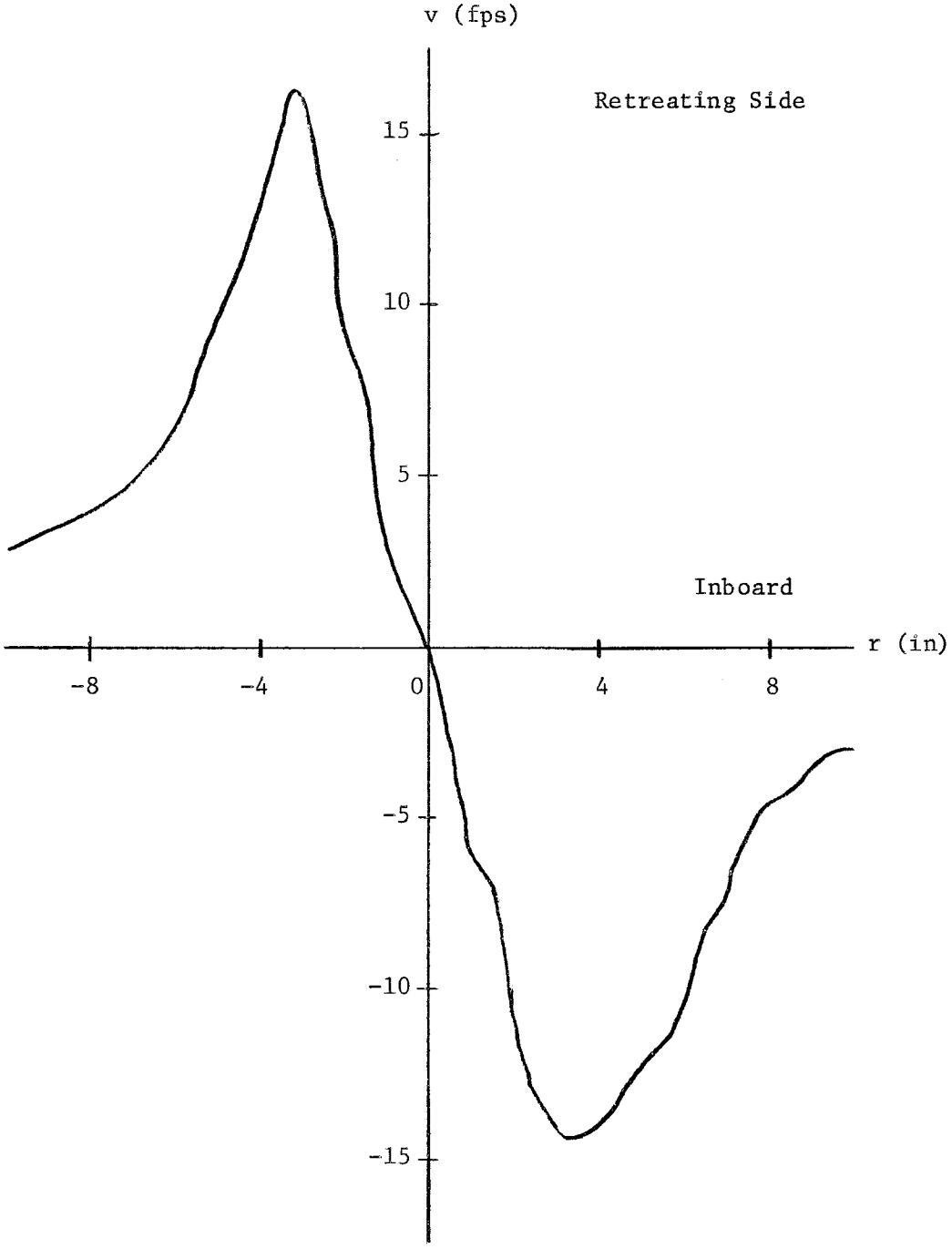


Figure 18(a). Faired Tangential Velocity Field Behind Rotor (Core Centered) x/R = 3.55 $\mu$ = .1285. Retreating Side

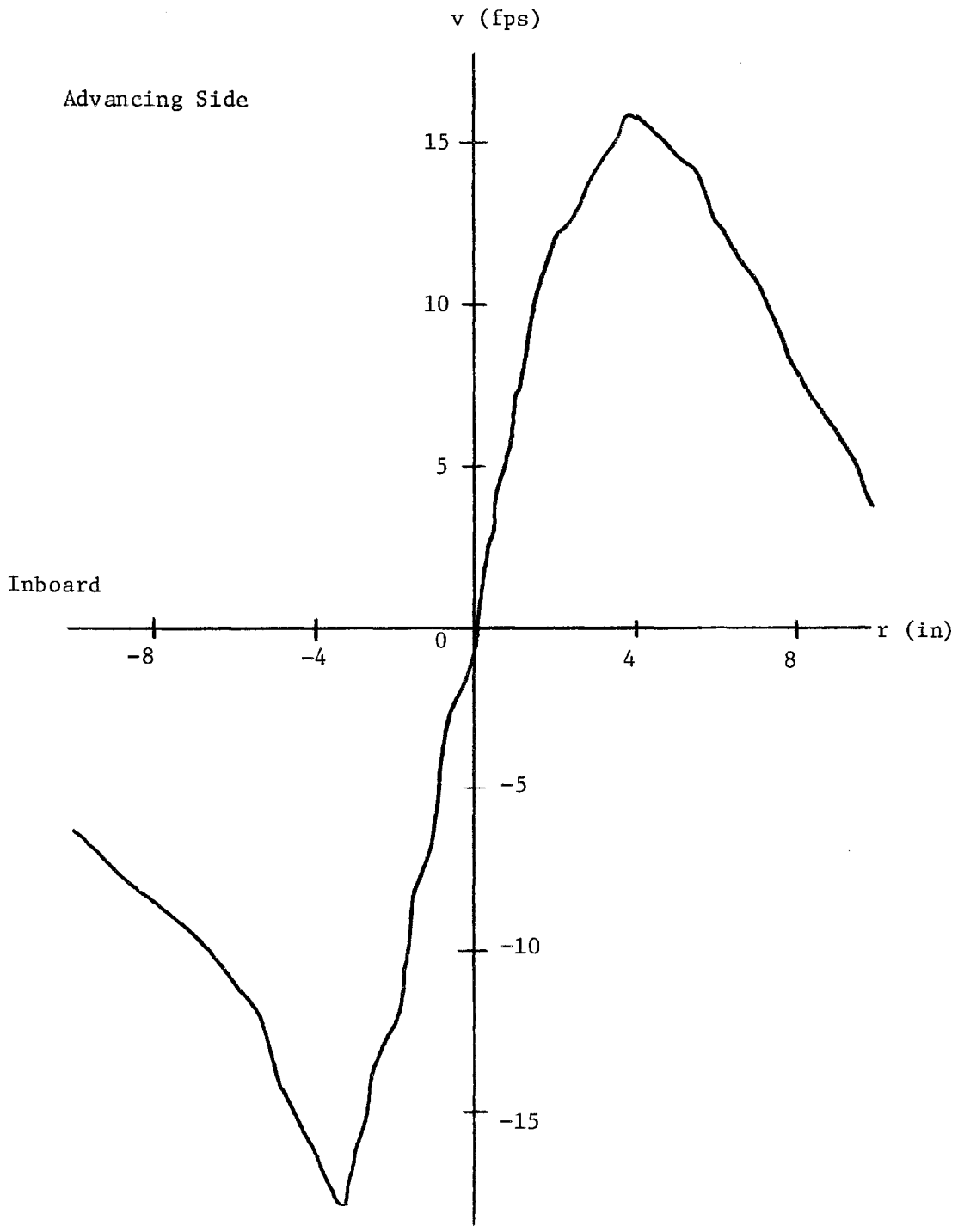


Figure 18(b). Faired Tangential Velocity Field Behind Rotor (Core Centered) x/R = 3.55 μ = .1285. Advancing Side

velocities at the core were used. The information obtained from Heyson's study is listed in Table 2.

Figure 19 is a plot of core radius versus tip speed ratio for both the data taken by Heyson[11] and that obtained by the author. Equation (9) predicts that the core radius should be independent of tip speed ratio, and only a function of whether the vortex system is laminar or turbulent. The results of Figure 19 suggest that this is the case since the larger rotor exhibits the smaller relative core size. However, there is a tendency for the core radius to decrease in size for both rotors as the tip speed ratio increases.

Figure 20 is a plot of the constant k defined by equation (3) for the experimental data obtained based on the circulation measured at the core radius and the estimated total circulation of the rotor. As can be seen from Figure 20 the smaller model resulted in higher k values than those obtained from Heyson's measurements. In both cases the derived k values appear to be high, particularly in view of the fact that the values for the small model are greater than unity.

Figure 21 is a plot of the measured maximum induced tangential velocities divided by the thrust coefficient and tip speed versus tip speed ratio. Equation (6) is also plotted on this figure. The relationship as expressed by equation (6) is,

$$\frac{v_i}{V_T C_T} = \frac{1.4}{\mu}$$

The least squares fit of the data to the parameters involved in equation (6) yielded the following relationship,

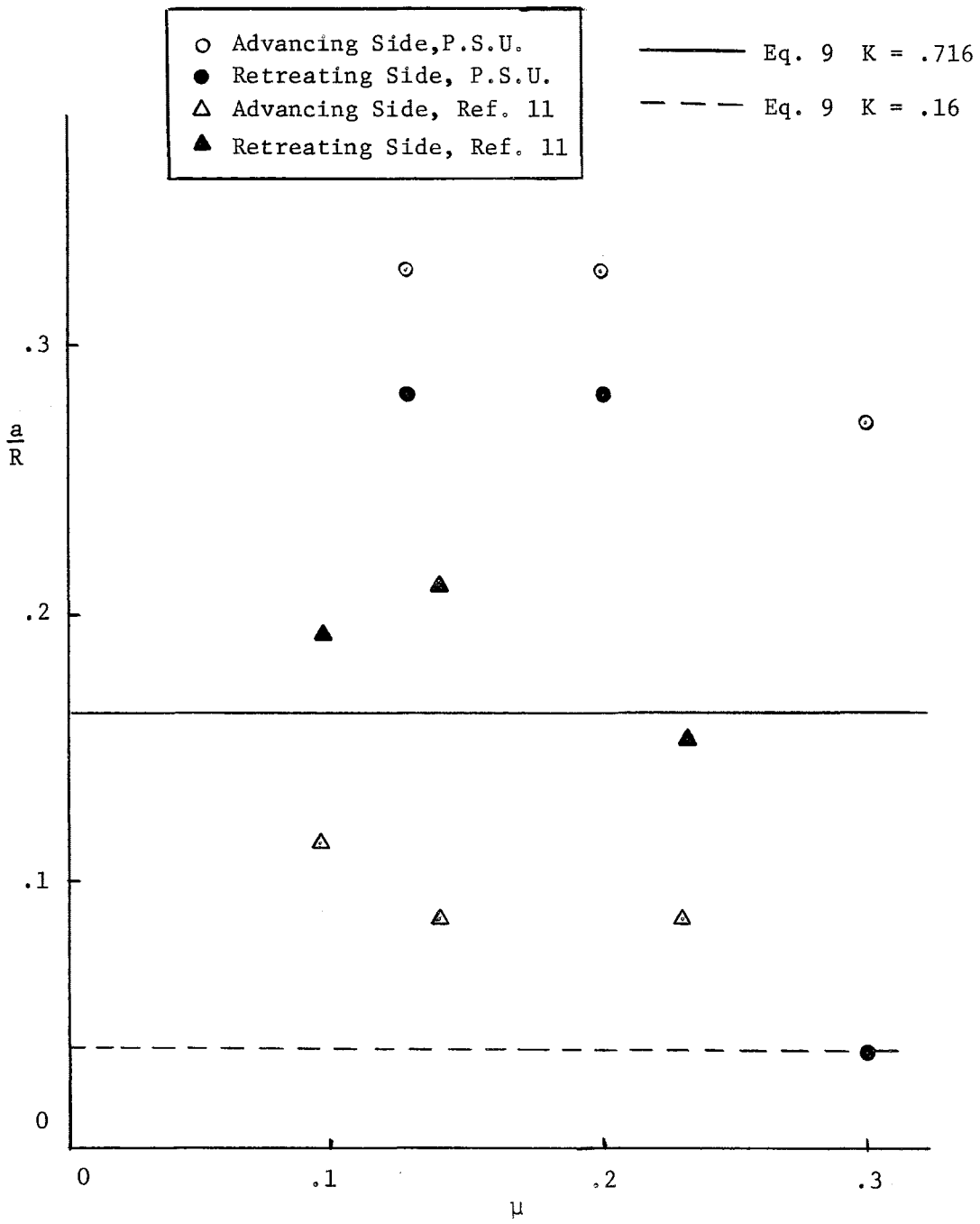


Figure 19. Core Radius vs. Tip Speed Ratio.

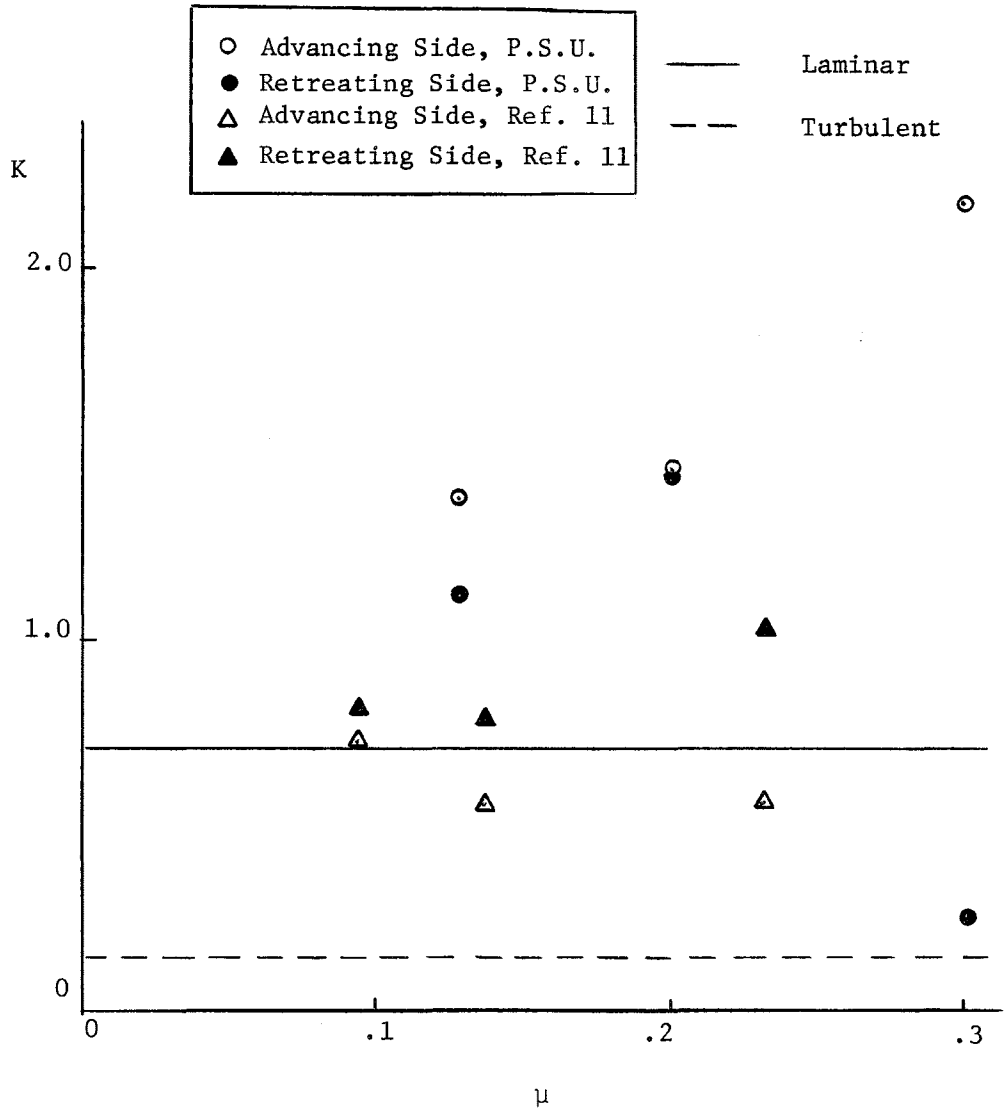


Figure 20. Ratio of Circulation at Core Radius to Total Circulation vs. Tip Speed Ratio.

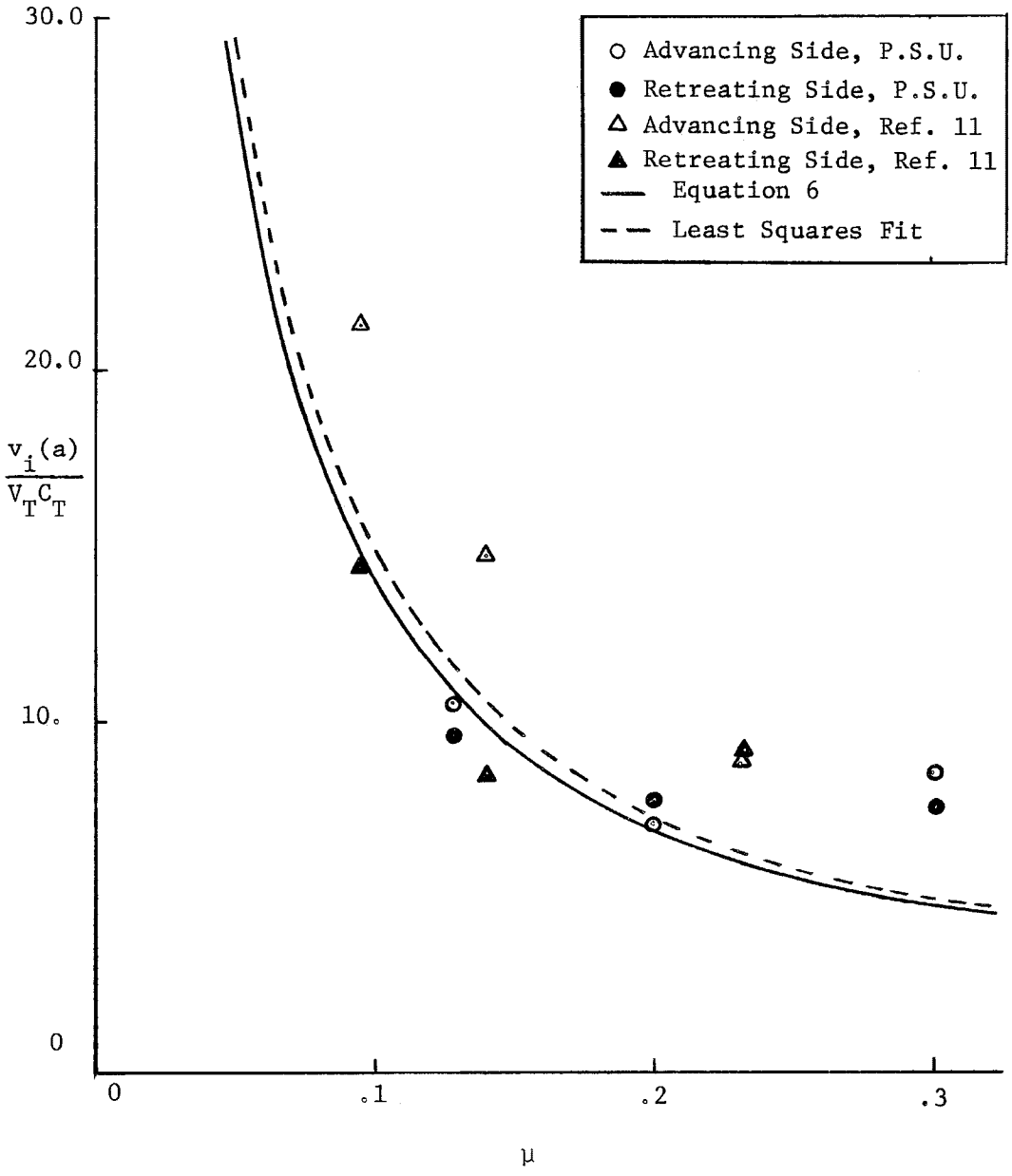


Figure 21. Maximum Induced Tangential Velocity vs. Tip Speed Ratio for Rotor Data.

Table 1. Data Taken at The Pennsylvania State University.

| Case No. and Side | $\mu$ | $V_T$ (fps) | V (fps) | $v_i$* (fps) | a (in) | $C_T$ | $\Gamma(a)$ ($f^2ps$) | $\Gamma_\infty$ ($f^2ps$) |
|---|---|---|---|---|---|---|---|---|
| 1 Adv. | .1285 | 144.0 | 18.5 | 16.9 | 3.6 | .0112 | 31.86 | 23.06 |
| 1 Ret. | | | | 15.5 | 3.2 | | 25.97 | |
| 2 Adv. | .201 | 129.5 | 26.0 | 12.3 | 3.6 | .0134 | 23.19 | 15.81 |
| 2 Ret. | | | | 13.5 | 3.2 | | 22.62 | |
| 3 Adv. | .301 | 86.4 | 26.0 | 11.5 | 3.0 | .0157 | 18.06 | 8.285 |
| 3 Adv. | | | | 10.2 | 0.4 | | 2.14 | |

* Averaged Over Inboard and Outboard Side of Each Core

Table 2. Data Taken by Heyson, Reference 11.

| Case No. and Side | $\mu$ | $V_T$ (fps) | V (fps) | $v_i$* (fps) | a (ft) | $C_T$ | $\Gamma(a)$ ($f^2ps$) | $\Gamma_\infty$ ($f^2ps$) |
|---|---|---|---|---|---|---|---|---|
| 1 Adv. | .095 | 500 | 47.5 | 34.1 | .855 | .0032 | 183.0 | 253.0 |
| 1 Ret. | | | | 23.0 | 1.434 | | 207.0 | |
| 2 Adv. | .140 | 500 | 70.0 | 27.4 | .645 | .0037 | 110.5 | 199.0 |
| 2 Ret. | | | | 15.7 | 1.575 | | 155.4 | |
| 3 Adv. | .232 | 450 | 104.5 | 12.7 | .645 | .0032 | 51.4 | 93.3 |
| 3 Ret. | | | | 13.4 | 1.15 | | 96.3 | |

* Averaged Over Inboard and Outboard Side of Each Core

$$\frac{v_i}{V_T C_T} \simeq \frac{1.48}{\mu}$$

This is close to the prediction of equation (6), even though the equation was based on a wing with an aspect ratio of 2.

# CHAPTER VI

## CONCLUSIONS AND DISCUSSIONS

From the analyses and empirical measurements performed in this study, it appears that the far field wake of a rotor can be adequately described by treating the rotor as a circular wing. As a result, the following relationships were found to be valid:

1. The maximum induced tangential velocity about a trailing vortex from a rotor is proportional to the product of the thrust coefficient and tip speed divided by the tip speed ratio. The constant of proportionality is approximately 1.48. The maximum tangential velocity is essentially the same as that which one would obtain by treating the rotor as a low aspect ratio fixed wing.

2. The size of the core radii of the trailing vortices of the rotor system is proportional to the rotor radius, and appears to be independent of other operating conditions. The constant of proportionality is a function of the nature of the vortex system, i.e. whether the flow in the vortex is laminar or turbulent. This behavior for core radii size is similar to the fixed wing core radius size behavior which is proportional to the mid-span chord of the wing, in that the rotor radius is proportional to the mean chord of a circular wing.

3. The large and small scale rotors exhibit scale effects with regard to the circulation at the core radius. It appears that the trailing vortex geometry for small scale rotors can be modeled by decay laws based on the Navier-Stokes equations while the trailing vortex of the large scale rotor is more accurately modeled by a logarithmic

circulation model incorporation empirical decay laws for fixed wing aircraft as described by reference 2.

# REFERENCES


1. Wetmore, J. W., and Reeder, J. P., "Aircraft Vortex Wakes in Relation to Terminal Operations," NASA TND-1777, April, 1963.

2. McCormick, B. W., Tangler, J. L., and Sherrieb, H. E., "Structure of Trailing Vortices," Journal of Aircraft, Vol. 5, No. 3, May-June, 1968.

3. Hoffmann, E. R., and Joubert, P. N., "Turbulent Line Vortices," Journal of Fluid Mechanics, Vol. 16, pp. 395-411, 1963.

4. Spreiter, J. R., and Sacks, A. H., "The Rolling Up of the Trailing Vortex Sheet and its Effect on the Downwash Behind Wings," Journal of Aeronautical Sciences, Vol. 18, No. 1, pp. 21-23, January, 1951.

5. Lehman, A. F., "Model Studies of Helicopter Rotor Flow Patterns," USAAVLABS Technical Report 68-17, April, 1968.

6. Landgrebe, A. J., "An Analytical Method for Predicting Rotor Wake Geometry," AIAA Paper # 69-196.

7. Heyson, H. H., "Analysis and Comparison with Theory of the Flow Field Measurements Near a Lifting Rotor in the Langley Full Scale Tunnel," NACA TN 3691.

8. Crimi, P., "Prediction of Rotor Wake Flows," CAL/USAAVLABS Symposium Proceedings, Vol. I Propeller and Rotor Aerodynamics, June, 1966.

9. Simons, I. A., Pacifico, R. E., and Jones, J. P., "The Movement, Structure and Breakdown of Trailing Vortices from a Rotor Blade," CAL/USAAVLABS Symposium Proceedings, Vol. I Propeller and Rotor Aerodynamics, June, 1966.

10. Lehman, A. J., "Test Section Size and Influence on Model Helicopter Rotor Performance," USAAVLABS Technical Report 71-6, March, 1971.

11. Heyson, H. H., "Induced Velocities Near a Lifting Rotor with Nonuniform Disk Loading," NACA TR 1319.

12. Connor, A. B., and O'Bryan, "A Brief Evaluation of Helicopter Wake as a Potential Operational Hazard to Aircraft," NASA TND-1227, March, 1962.

13. Grow, T. L., "The Effect of Wing Geometry and Lower Surface Boundary Layer on the Rolled-Up Tip Vortex," M.S. Thesis, The Pennsylvania State University, 1967.

14. Eisenhuth, J. J., and McCormick, B. W., "An Observation on the Vortex System of Dual-Rotation Propellers," Journal of Aeronautical Sciences, Vol. 20, No. 6, September, 1953.

15. Gessow, Alfred, and Myers, G. C., Jr., Aerodynamics of the Helicopter. New York: Fredrick Ungar Publishing Co., 1952.

16. McCormick, B. W. Aerodynamics of V/Stol Flight. New York: Academic Press, 1967.

17. DISA Electronics and Service Manual for Type 55005 Battery Operated CTA. DISA Electronics A/S, Herlev, Denmark.

# APPENDIX I

## Basic Principle of the Constant Temperature Hot-Wire Anemometer[17]

The hot-wire anemometer works on the principle that a thin electrically heated wire, suspended between two prongs, conducts heat to the fluid surroundings. The heat transfer from the wire obeys the two-dimensional heat transfer relationship for a cylinder as described by L. V. King. The formula, known as King's Law, states that the rate of heat loss of the wire, Q, is related to the fluid velocity U by the following relationship:

$$Q = (T - T_o)(A_1 + B_1 u^{1/2})$$

where T is the wire operating temperature, $T_o$ is the fluid temperature, and $A_1$, $B_1$ are empirical constants.

The rate of heat loss must equal the power generated, P, in the wire by the electric current, I, when the wire is held in thermal equilibrium. That is,

$$P = I^2R;\ T - T_o = \text{constant}$$

where R is the wire operating resistance.

Under thermal equilibrium conditions

$$R = R_o\ (1 + \alpha\ (T - T_o)\ )$$

where $R_o$ is the resistance of the wire at fluid temperature and $\alpha$ is a constant of proportionality. Thus, King's Law can be rewritten as

$$\frac{I^2R}{R-R_o} = A_2 + B_2 \; u^{1/2}$$

This relationship has been found to be valid in atmospheric air at velocities in the range of .5 m/sec to 100 m/secs.

A feedback system keeps the wire temperature constant with the output signal being a voltage E which obey's King's Law in the following form:

$$E^2 = A + B \; u^{1/2}$$

The hot-wire is sensitive only to velocities normal to the wire. If the wire axis is inclined from the direction of the flow velocity by an angle $\theta$, then the relationship becomes:

$$E^2 = A + B \; u'^{1/2}$$

where

$$u' = u \sin \theta$$

For a two-dimensional flow u' becomes

$$u' = V \sin \theta + u \cos \theta$$

if $V$ is a constant, then u can be easily measured with the hot-wire. The final relationship for u as a function of E and the empirical constants A and B is then:

$$u = \csc \theta \left\{\left[\frac{(E^2-A)}{B}\right]^2 - V \sin \theta\right\}$$

Figure 22 illustrates the geometry of the hot-wire probe as applied to a two-dimensional flow with one vector component constant.

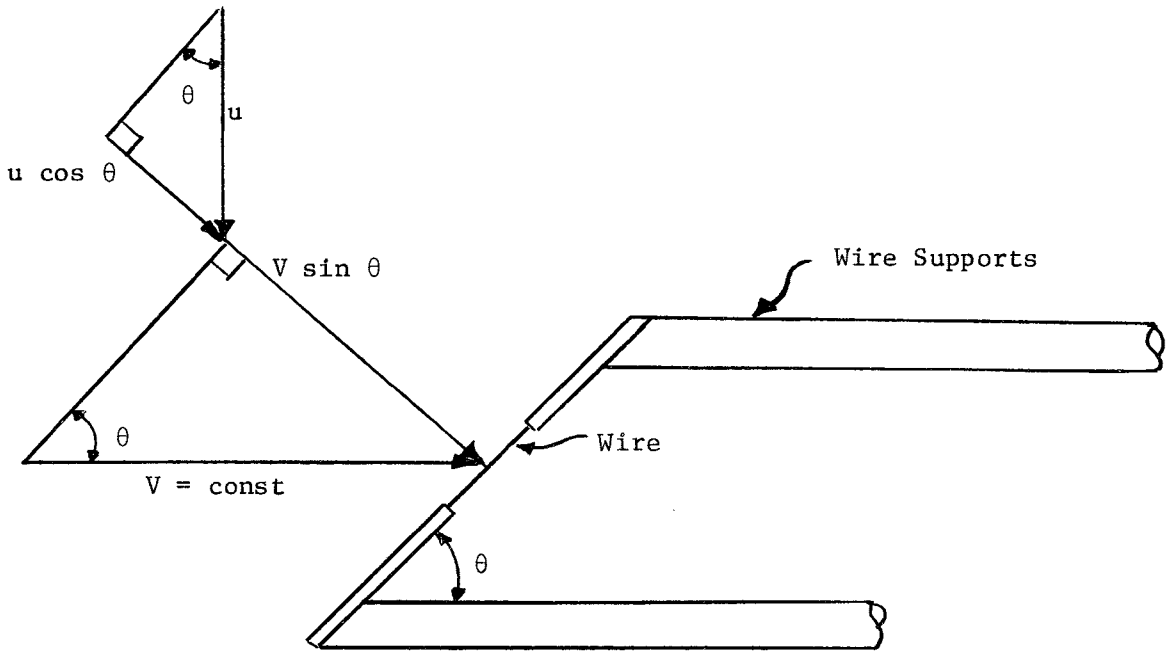


Figure 22. Hot-Wire and Two-Dimensional Flow Geometry.

# APPENDIX II

## Truncation of $\psi$

Because it is necessary to integrate equation (38) numerically with a digital computer, a method for defining the length of vortex system necessary to obtain solutions approaching solutions of the infinite system is required. The following method of defining a satisfactory, finite length was used.

Consider an infinite vortex filament with constant strength. From the Biot-Savart Law the velocity at any radial distance from the filament is

$$v(h) = \frac{\Gamma}{4\pi R}\frac{2}{h}$$

where $h = \frac{r}{R}$. For a finite length filament the velocity is just:

$$v(h) = \frac{\Gamma}{4\pi R}\frac{\cos\gamma + \cos\beta}{h}$$

The error in the velocity calculation due to using a finite length in place of an infinite length filament would be

$$E = 1 - \frac{\cos\gamma + \cos\beta}{2}$$

For simplicity consider only the case where the limits on the finite length filament are symmetrical about the point of interest, then $\cos\gamma = \cos\beta$, therefore

$$E = 1 - \cos\gamma$$

From Figure 23 it can be seen that:

$$\cos \gamma = \frac{\ell}{\sqrt{\ell^2 - h^2}}$$

where $\ell$ is a non-dimensional length. This yields:

$$E = 1 - \frac{\ell}{\sqrt{\ell^2 - h^2}}$$

Solving for $\ell$ as a function of h and the desired error yields:

$$\ell = \frac{h\ (1 - E)}{\sqrt{2E^2 - E^2}}$$

For the symmetrical case the total segment length must be $L = 2\ell$. For a desired accuracy this segment length is then used for the limiting length on the numerical integration. This length, $\ell$, in turn can be directly related to the angle $\psi$ with the use of equation (14) to obtain an integration limit on $\psi$. For this study an error of 5 % was deemed acceptable.

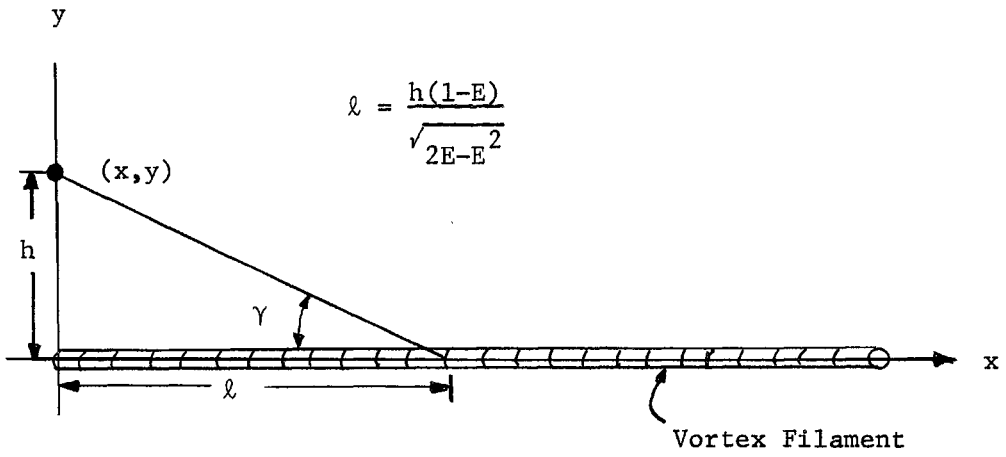


Figure 23. Geometry for Calculation of Vortex Filament Cutoff Length.

# APPENDIX III

## Sample Data Reduction

From Table 1, the tip speed ratio is

$$\mu = V/V_T = 18.5/144.0 = .1285$$

For the NACA 0012 airfoil the slope of the lift curve is approximately

$$a_o \simeq 5.73\ C_\ell/\text{rad}$$

The solidity for this rotor is

$$\sigma = Bc/\pi R = (2)(2")/\pi(11") = .11575$$

The non-dimensional hub radius is

$$h = 1.5"/11.0" = .1364$$

The hub collective pitch angle was $10^o$ or .174 radians.

With this information, the thrust coefficient for the teetering rotor can be found approximately by the following expression:

$$C_T = \frac{1}{2}\sigma a_o \theta_o \frac{\frac{1}{3}(T_B^{\,2} - h^3) + \frac{1}{2}(T_B - h)\mu^2}{1 + \frac{T_B^{\,2} - h^2}{8}\frac{a_o\sigma}{\mu}}$$

or for this particular case,

$$C_T = .01122$$

Therefore, the total circulation for the far field vortes should be

$$\Gamma_\infty = 2\ C_T\ RV_T/\mu = 23.06\ ft^2/sec.$$

On the advancing side the following measured values were obtained:

$$v_i = 16.9\ fps$$

$$a = 3.6"$$

Therefore, the circulation at the core radius is

$$\Gamma(a) = 2\pi a v_i = 31.86\ ft^2/sec.$$

On the retreating side the following measured values were obtained:

$$v_i = 15.5\ fps$$

$$a = 3.2"$$

Therefore, the circulation at the core radius is

$$\Gamma(a) = 25.97\ ft^2/sec.$$

The k values for this case are 1.38 and 1.13 for the advancing and retreating sides respectively.